TOPOLOGICAL PHOTONIC CRYSTAL RING RESONATORS

Alexis Hotte-Kilburn

A thesis

in

The Department

of

Physics

Presented in Partial Fulfillment of the Requirements
For the Degree of Master of Science (Physics)
Concordia University
Montréal, Québec, Canada

January 2021

CONCORDIA UNIVERSITY
School of Graduate Studies

This is to certify that the thesis prepared

By: **Alexis Hotte-Kilburn**

Entitled: **Topological Photonic Crystal Ring Resonators**

and submitted in partial fulfillment of the requirements for the degree of

Master of Science (Physics)

complies with the regulations of this University and meets the accepted standards with respect to originality and quality.

Signed by the final examining commitee:

_____ Chair

_____ Dr. Saurabh Maiti _____ Examiner

_____ Dr. Alexandre Champagne _____ Examiner

_____ Dr. Pablo Bianucci _____ Supervisor

Approved _____

Dr. Valter Zazubovits, Graduate Program Director

_____ 2021   _____

Pascale Sicotte, Ph.D., Dean

Faculty of Arts and Science

Abstract

Topological Photonic Crystal Ring Resonators

Alexis Hotte-Kilburn

Concepts of topology arise in condensed matter physics when considering states at the boundary of a periodic structure. Recently, there has been interest in exploring topology in optical contexts. Optics is an excellent platform to study these effects, due to the high degree of control over the geometry and material. The simplest example of a model exhibiting topological properties is the Su-Schrieffer-Heeger (SSH) chain, where an extra periodicity (also known as dimerization) is added to a photonic crystal waveguide. By creating sites where the dimerization changes abruptly, it is possible to create topological edge states, which confines resonant modes that are protected from imperfections.

Here, we study the SSH model in a ring resonator, where a dimerized photonic crystal waveguide loops in on itself. The dispersion relations of various waveguides are first calculated using a frequency domain approach. By using those waveguide unit cells as the elements to construct phase transitions, the properties of those resonant modes and the extent of topological protection will be studied by adding random variations to the holes of the unit cells. Simulations show that topological protection of the quality factors hold for 7.8% variation in the hole radii. The loss mechanisms of these optical cavities will also be analyzed to confirm topological protection of the lattice. At last, we then discuss how these ring resonators can be fabricated and experimentally studied on a silicon chip.

Acknowledgments

First and foremost, I would like to thank my thesis advisor, Prof. Pablo Bianucci, for giving me the opportunity to study in the field I am passionate about, and for introducing me to the world of photonics. His coaching, kindness and expertise have made my time during my masters both an enjoyable and instructive one. I am grateful to have had to opportunity to work in his group, and look forward to continuing my studies with him.

I would also like to thank my fellow cohorts: Kathleen, Mathieu, Rajni, and Samar, for accepting me into the group, for the interesting discussions, and for the help you have all given me. I wish you all success in your future careers.

As well, thank you to my sister, Valerie, for all those years of friendships and for the many laughs we've shared.

Finally, I would like to thank both my parents, Sophie and Laurent, for endlessly supporting me during my studies. Their encouragement and love have allowed me to reach heights I never thought to be possible. Thank you for believing in me when I didn't, and for being my number one fans. Their proofreading of this thesis also proved to be immensely valuable!

Contents

List of Figures

List of Tables

Chapter 1

Introduction

Electronic circuits are no doubt one of most important pieces of technology in our society, being responsible for many inventions, such as the digital computer and medical equipment. While its uses cannot be understated, fundamental limitations in electronics exists which may limit its applications in other domains. For example, data transmission is copper cables is severely limited by distance, due to the signal's attenuation. In addition, overheating of devices is still a problem, which may limit their usefulness under a certain load.

Electronic circuits use the electron to process and transform signals. On the other hand, photonic integrated circuits can instead use a photon as a signal. A common example of a photonic device which processes photons is the optical fiber, used in telecommunications. By guiding light in the cable's core, some of the highest data bandwidths can be conceived [1]. In order for photonic devices and circuits to become more widely adopted, ways to control the light's propagation must be devised.

One promising device to modify an optical signal is the microresonator, a cavity which can be used to trap particular frequencies of light, called resonances. By carefully engineering the shape and dimensions of the resonator, we can have precise control of which wavelengths become resonances. As such, it can act as a kind of 'filter' for light. Resonances have many applications of technological importance, including sensitive bacterial sensing [2], and complex filters [3].

An important type of optical resonator which can be integrated on a chip is the

microring resonator [4]. Like an optical fiber, it can guide light along a circular path in a higher index core. Under certains conditions and for particular wavelengths of light, a wave propagating around a ring will result in a resonance, where the core will have a high buildup of energy. When a microring has a resonance, these modes of light can be made to have high field amplitudes. Nevertheless, there exist loss mechanisms in optical microring resonators, which affects how long-lived the resonances will be. While high quality resonances have narrow dips in its spectral profile, the presence of loss can widen the resonances, which will negatively affect the performance of the resonator.

As a way to fabricate photonic circuits, we can leverage existing technologies conceived for the electronic circuits. Indeed, existing silicon manufacturing processes can be directly applicable to the fabrication of photonic devices on a chip. As such, the research resources applied to microelectronics fabrication are readily available for commercial foundries. An important platform to arise is the silicon-on-insulator. This platform uses a thin (typically 220 nm) layer of silicon on top of a silicon wafer as a substrate, with 2000 nm of silicon dioxide on it. It is on this layer where the silicon devices can be etched by state-of-the-art lithography processes [5]. This grants us complete control over the device's geometry to construct waveguides, couplers, resonators, and Mach-Zehnder interferometers [6].

However, a major obstacle that stands in the way of having high quality photonic integrated circuits is the introduction of nanoscale fabrication defects during the etching process of lithography. These defects, by introducing additional scattering of light, results in propagation loss for optical waveguides and fibers, and a lower Q-factor in resonators. For applications where great sensitivity is required, this may compromise the performance of these devices. It would be of great interest for circuit designer to fabricate components whose parameters are insensitive to those perturbations.

To counter this effect, condensed matter physicists have devised electronic devices which takes advantage of the sample's topology, a property that explains how a system can be continuously deformed without closing a bandgap [7]. A physical consequence of topology is that the crystal's boundary can tolerate small perturbations (to the extent that its bandgap is not closed) and still support an unperturbed current (which are said to be topologically protected). Physically, we can realize these states by

taking two materials of a different topological invariant and creating an interface between them [8].

In addition, we can take advantage of the mathematical parallels that can be made between the equations of quantum mechanics and electromagnetics. While topology may be traditionally thought to be a phenomena that arises in quantum condensed matter, one can nevertheless implement topology in optical contexts. This implies that we can construct an interface between two materials of different topological invariant and still retain topological protection, even with lithography fabrication roughness. This can result in an undisturbed propagation of light in a waveguide array, or resonators which retain their high Q-factor mode profiles in the presence of perturbations. In optics, we can artificially introduce topology to a periodic system by introducing a magnetic field to break time-reversal symmetry [9]. However, this can make the experimental study of these devices more challenging, due to the magneto optical effect. A simpler way would be to engineer the device's geometry by constructing an interface between two periodic structures, such as in an array of devices. Clearly, this allows for great control over the device's properties, which makes optics an excellent platform to study topology.

In this project, we propose to study the Su-Shrieffer-heeger (SSH) model [10], one of the simplest models which can show properties of topology, in an optical context. The SSH models can be made by taking a chain of sites and having an alternating hopping strength/coupling distance, which dimerizes the lattice. By taking a waveguide and periodically patterning an array of holes along it, we can also construct an interface that supports a topological edge state, by connecting two different waveguides with different dimerizations. To also implement a periodic boundary condition on the chain, the SSH model will be superimposed on a standard ring resonator. This thesis will aim to study, by means of numerical simulations, the properties of such a system, including the dependence on various geometrical parameters, and the extent of topological protection.

This thesis will begin by reviewing the fundamentals concepts of integrated optical devices in Chapter 2, including the waveguide and resonator. This chapter will also explore the phenomena which allows these devices to operate in an integrated circuits, namely with total internal reflection to keep light confined, and coupled-mode theory,

which explains energy exchange occurs between two or more optical devices. In chapter 3, we will explore ways to control the propagation of light in periodic structures, as well as highlight the similarities and differences between compared to quantum condensed matter. By taking those mathematical analogies into consideration, chapter 5 will explore topology in detail, including the arisal of the topological invariant and systems which have been implemented in optics. The core off this work, chapter 6, will show the simulation results of the SSH model in a ring resonator, including the proposed designs to be studied. In particular, we showed, by introducing artificial perturbations, that the cavity formed in this system could sustain its Q-factors, which implies that the light is immune to the loss introduced. Finally, chapter 7 will highlight some practical considerations of the fabrication of photonic circuits, as well as a proposed experimental scheme.

Chapter 2

Guided and confined electromagnetic waves

A key property of photonic integrated circuit is the ability be able to store and guide light along the components for signal processing purposes. To achieve this, both optical resonators and optical waveguides are used, respectively. By trapping a beam of light in a high index of refraction material, the main mechanism to control the propagation of light, total internal reflection, can be used to construct photonic devices. In this chapter, we will focus our attention on the phenomenon of total internal reflection, along with the most fundamental optical devices: the slab waveguide and the whispering-gallery mode resonator. Then, we will consider the coupling of adjacent modes from those devices by a reciprocity approach.

2.1   Total internal reflection

To better study optical devices, we must study how rays travel at an interface between 2 materials, with indices of refraction n_1 and n_2. A ray approaching the interface between the 2 interfaces will either be fully reflected, be partially reflected and transmitted, or be partially reflected and travelling along the interface [11]. For a given pair of materials, Snell's law can be used to calculate at which angles the ray is transmitted:

$$n_1 \sin \theta_i = n_2 \sin \theta_t \tag{1}$$

With θ_t and θ_i being the transmitted and incident angles of the ray.

A necessary condition for the transmitted ray to travel parallel to the interface is $n_1 > n_2$ and $\theta_t > 90°$. With this, we can define a critical angle for the materials as:

$$\theta_c = \arcsin\left(n_1/n_2\right) \tag{2}$$

For incident angles $\theta_i > \theta_c$, all incoming light will be reflected back into n_1, while if $\theta_i < \theta_c$, a portion of the light will be transmitted to the medium beyond. In the former case, all of the energy will be confined to the higher index material.

While no energy could be transmitted in the case of a fully reflected ray, there would nevertheless an electromagnetic field found in the lower index medium close to the interface. This wave, also known as an evanescent wave, travels along the parallel of the interface, and exponentially decays to negligible values a few wavelengths away.

To see the form of the field of an evanescent wave, we consider the electric field of the transmitted ray and apply Snell's law. By assuming that the field's envelope is modulated by a frequency and spatial term as it travel,s we can write the transmitted component as:

$$\vec{\mathbf{E}}_t = \vec{\mathbf{E}}_{0t} \exp i\left(\vec{\mathbf{k}}_t \cdot \vec{\mathbf{r}} - \omega t\right) \tag{3}$$

With $\vec{\mathbf{k}}_t$ being the field's wave-vector, indicating the propagation direction. By applying the geometry of the ray, we can rewrite the components of the wave-vector as:

$$\begin{aligned} k_{tx} &= k_t \sin \theta_t \\ k_{ty} &= k_t \cos \theta_t \end{aligned} \tag{4}$$

By using Snell's law to the transmitted angle and restricting ourselves to $\sin \theta_i > n_2$ we have:
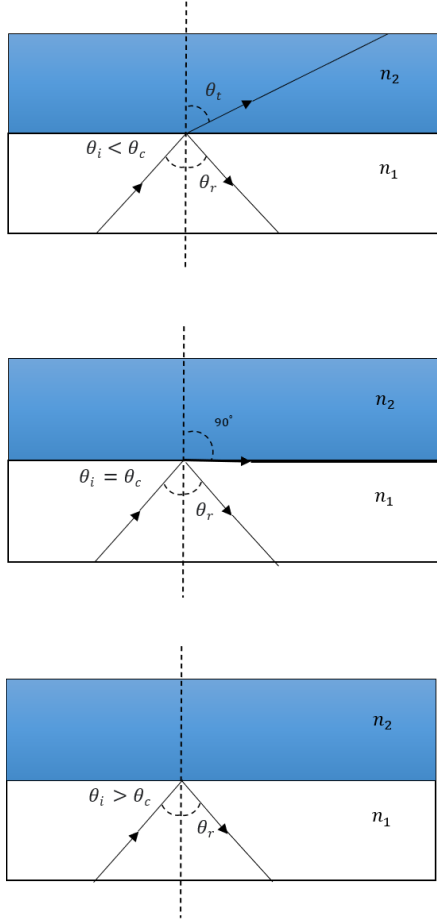
Figure 1: Total internal reflection for the three cases of incident angles, when the incident ray being being transmitted to the medium beyond, when the transmitted ray is parallel to the interface, and when the ray is totally internally reflected.

$$
\begin{aligned}
k_{ty} &= \pm i k_t \left(\frac{\sin^2 \theta_i}{n_2^2} - 1 \right)^{1/2} \\
k_{tx} &= \frac{k_t}{n_2} \sin \theta_i
\end{aligned}
\tag{5}
$$

Where we have defined β to be the electromagnetic wave's propagation constant, in the y direction.

$$
\overrightarrow{\mathbf{E}}_t = \overrightarrow{\mathbf{E}}_{0t} e^{\mp \beta y} e^{i(k_t x \sin \theta_i / n_2 - \omega t)}
\tag{6}
$$

This result implies that the wave's amplitude will decrease exponentially as it gets reflected off a lower index material. Finally, while the wave's amplitude does not vary upon reflections, there is a phase shift, known as the Goos-Hänchen shift [12], where

the ray will experience a small lateral shift from the position where the beam strikes at interface. The field amplitudes can be described accordingly as:

$$E_r = E_i e^{2i \frac{\sqrt{n_1^2 \sin^2 \theta_i - n_2^2}}{n_1 \cos \theta_i}} \tag{7}$$

2.2 Dielectric optical waveguides

A dielectric waveguide is a structure that uses total internal reflection to guide a ray along a particular direction. A slab waveguide is constructed by putting a high index core material layer, n_{core}, in between a cladding and substrate layers, $n_{clad.}$ and $n_{subs.}$. By repeatedly striking the 2 interfaces, the ray will be reflected back and forth and guided along the core. The three slabs are made to be of infinite extent in the $\hat{y}$ and $\hat{z}$ directions.
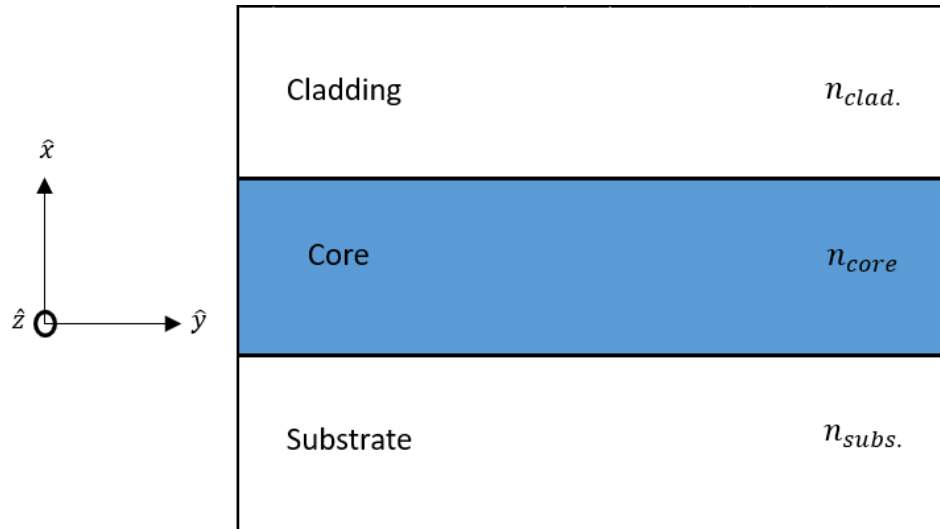
Figure 2: A typical dielectric slab waveguide arrangement, showing a core of high index, n_{core}, surrounded by a lower index substrate $n_{subs.}$ and cladding $n_{clad.}$.

For guiding to occur, the ray must obey two critical angle conditions; the substrate, and the cladding. These critical angles are written as:

$$\theta_{c1} = \arcsin\left(n_{clad.}/n_{core}\right)$$
$$\theta_{c2} = \arcsin\left(n_{subs.}/n_{core}\right) \tag{8}$$

Just as before, we now impose that $n_{core} > n_{clad.}$ and $n_{core} > n_{subs.}$ for the material's indices of refraction. In addition, the ray's incident angle must also obey $\theta_i > \theta_{c1}$ and $\theta_i > \theta_{c2}$. Otherwise, the light will radiate into the cladding or substrate.
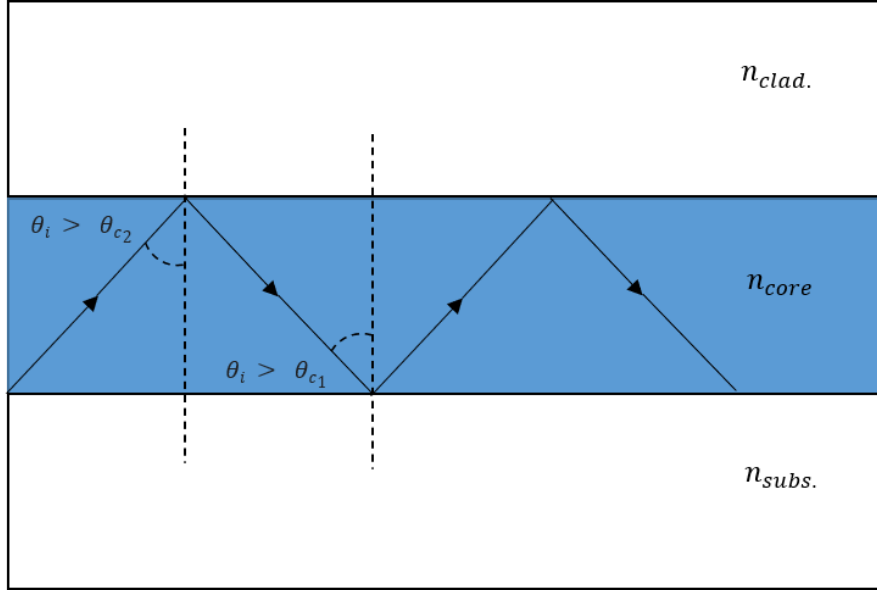
Figure 3: An example of a ray being continuously reflected between two interfaces in a dielectric slab waveguide. The ray's incident angle must be greater than both of the critical angles.

The following will present a boundary-value problem approach to the field analysis of a slab waveguide [13]. In order to quantify the propagating modes in an optical waveguide, we resort to Maxwell's equations to begin our analysis. In differential form, with charge density ρ and current sources J, they are written as:

$$
\begin{aligned}
\nabla \cdot \mathbf{E} &= \frac{\rho}{\varepsilon_0} \\
\nabla \times \mathbf{E} &= -\frac{\partial \mathbf{B}}{\partial t} \\
\nabla \cdot \mathbf{B} &= 0 \\
\nabla \times \mathbf{B} &= \mu_0 \varepsilon_0 \frac{\partial \mathbf{E}}{\partial t} + \mu_0 \mathbf{J}
\end{aligned}
\tag{9}
$$

Together, with appropriate boundary conditions, they allow us to solve a multitude of electromagnetic problems. In order to simplify our analysis of waveguides, we consider our region as being source free, that is, we set: $\rho = 0$ and $\mathbf{J} = 0$. This a reasonable assumption if we assume that the ray of light comes elsewhere. With this simplification, we now have:

9

$$\nabla \cdot \mathbf{E} = 0$$
$$\nabla \times \mathbf{E} = -\frac{\partial \mathbf{B}}{\partial t}$$
$$\nabla \cdot \mathbf{B} = 0 \tag{10}$$
$$\nabla \times \mathbf{B} = \mu_0 \varepsilon_0 \frac{\partial \mathbf{E}}{\partial t}$$

Next, in order to more easily solve these equations, we will decouple the equations such that they only contain one type of field. To decouple our fields, we can apply the curl operator to each curl term to obtain:

$$\nabla \times (\nabla \times \mathbf{E}) = \nabla \times \left(-\frac{\partial \mathbf{B}}{\partial t}\right) = -\frac{\partial}{\partial t}(\nabla \times \mathbf{B}) = -\mu_0 \varepsilon_0 \frac{\partial^2 \mathbf{E}}{\partial t^2}$$
$$\nabla \times (\nabla \times \mathbf{B}) = \nabla \times \left(\mu_0 \varepsilon_0 \frac{\partial \mathbf{E}}{\partial t}\right) = \mu_0 \varepsilon_0 \frac{\partial}{\partial t}(\nabla \times \mathbf{E}) = -\mu_0 \varepsilon_0 \frac{\partial^2 \mathbf{B}}{\partial t^2} \tag{11}$$

Then, by applying the $\nabla \times (\nabla \times \mathbf{A}) = \nabla(\nabla \cdot \mathbf{A}) - \nabla^2 \mathbf{A}$ vector identy on the curl-curl terms and removing the divergence terms, we are left with 2 uncoupled field equations, which are now of second differential order:

$$\mu_0 \varepsilon_0 \frac{\partial^2 \mathbf{E}}{\partial t^2} - \nabla^2 \mathbf{E} = 0$$
$$\mu_0 \varepsilon_0 \frac{\partial^2 \mathbf{B}}{\partial t^2} - \nabla^2 \mathbf{B} = 0 \tag{12}$$

These are also known as the electromagnetic wave equations. We can simplify our analysis if we make assumptions about the functional form of the electric field amplitude. Just as before, for the case of electromagnetic waves, we can modulate the field's amplitude by a modulating complex exponential in both time (with a frequency ω) and space (in the direction of guiding, with a propagation constant k_y). In two-dimensional systems, we must also specific the field's polarization. We can either have TE modes, where we are solving for the z transverse component of the magnetic field, or TM modes for the electric field. The following analysis will be for the case of TE polarized modes. With this information, the electric field takes the form of (in the core, cladding, and substrate):

$$E_z(x,y) = \hat{e}_z(x)e^{i(\omega t - k_y y)} \tag{13}$$

With the basic form of the electric field, we can substitute it into the electric field wave equation, to obtain simple differential equations (in the core, and both the substrate

and cladding regions, which will be made to have the same index of refraction for illustration purposes). Let us also map the index of refraction to the permitivity constant $n = \sqrt{\varepsilon \varepsilon_0 \mu \mu_0}$. Doing the aforementioned substitution leaves with simpler ordinary differential equations:

$$
\begin{aligned}
\frac{d^2 \hat{e}_z}{dx^2} - \alpha^2 \hat{e}_z &= 0 \\
\frac{d^2 \hat{e}_z}{dx^2} + k_x^2 \hat{e}_z &= 0
\end{aligned}
\tag{14}
$$

Which we have simplified by means of the following substitutions :

$$
\begin{aligned}
\alpha &= \sqrt{k_y^2 - \omega^2 \mu_0 \epsilon} \\
k_x &= \sqrt{\omega^2 \mu_0 \epsilon_{core} - k_y^2}
\end{aligned}
\tag{15}
$$
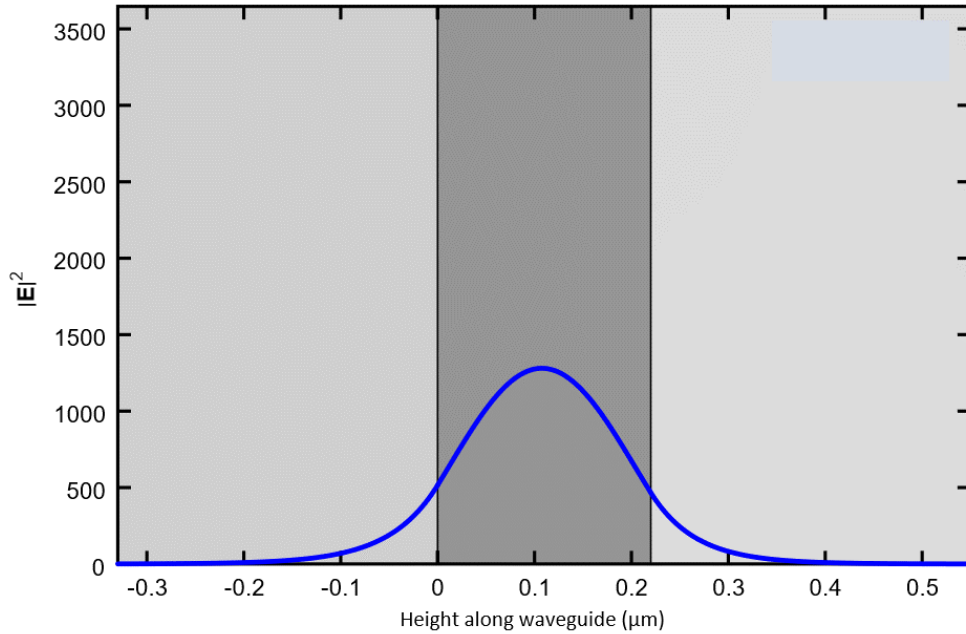
Figure 4: The optical confinement of the electric field in a dielectric slab waveguide. The light is clearly confined to the waveguide's core, denoted by the grey color.

To complete the solution, we must apply proper boundary condition of the system's geometry. At the 2 interfaces, the solutions of the electric field must match, as well as be continuous. By assuming that the thickness of the high index core is d, we can write the solution of these differential equations in the 3 regions as:

11

$$\hat{e}_z = \begin{cases} Ae^{-\alpha_x(x-d)}; d < x \\ A\frac{\cos k_x x}{\cos k_x d}; -d < x < d \\ Ae^{\alpha_x(x+d)}; x < -d \end{cases} \qquad (16)$$

Where A serves to simplify the algebra. With the fields in hand, what remains is to calculate for the waveguide's propagation constant, k_y for a given frequency ω. From the equation, it is simpler to start by finding α and k_x first. By applying the continuity condition and eliminating k_y from the previously defined substitutions, we obtain the expression:

$$\tan k_x d = \sqrt{\frac{\omega^2 \mu_0 \epsilon_{core} d^2}{(k_x d)^2}\left(1 - \frac{\epsilon}{\epsilon_{core}}\right) - 1} \qquad (17)$$

As the frequency is raised, an additional guided mode appears from $\tan k_x d$. Generally, this appears at frequencies such that the condition $k_x d = m\pi/2$ occurs, where m is an integer.

From the previous substitution, finding k_y as a function of the mode's frequency ω gives us:

$$k_y d = \sqrt{\omega^2 \mu_0 \epsilon_{core} d^2 - (k_x d)^2} \qquad (18)$$

By plotting the expression for the dielectric slab waveguide, we obtain its dispersion relation, or band diagram. This dispersion relation can give us insightful information about a waveguide's design. As previously hinted, there are only a discrete amount of modes that can exist in a particular waveguide's design (denoted by its integer, m, which corresponds to different solutions of equation 17). Those discrete modes can be seen from the dispersion relation by the individual curves. In practical cases, we are often interested in single-mode operation, where only the fundamental mode ($m = 0$) can exist in the waveguide. The field pattern of this fundamental mode has no nodes, whereas higher ordered modes have increasingly complex field patterns. In addition, the localization of light within the core tends to lessen as the mode's integer increases, which may increase the radiation loss. We can avoid exciting high ordered mode by keeping our waveguide dimension small enough.
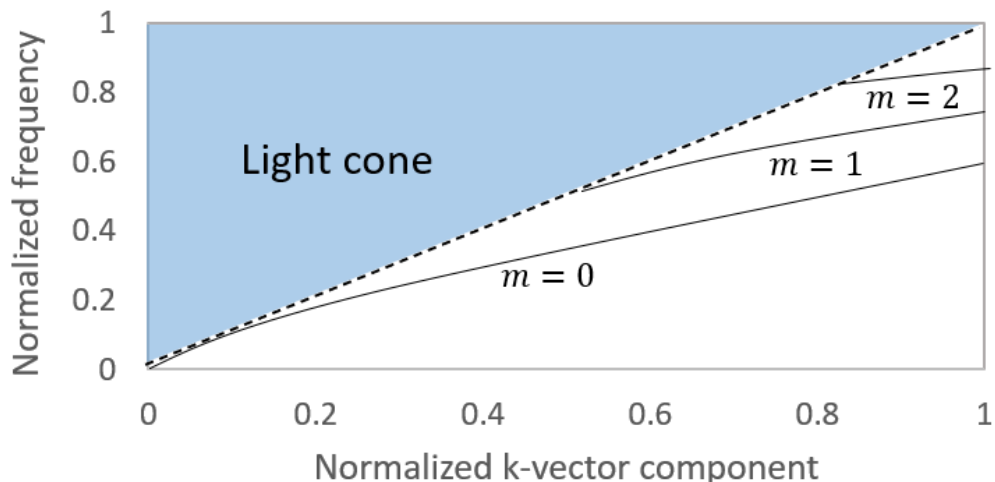
Figure 5: A qualitative graph of the dispersion relation of an optical waveguide. The main features include the region of radiating modes beyond the light cone, and the discrete bands for each integer numbered propagating mode.

As can be seen from the formula of the dispersion relation, there is a point where the square root cannot be evaluated for negatives arguments. Beyond, no guided modes can exist in the core, and the light will be radiated in the cladding and substrate. As we recall from the treatment of total internal reflection, for a ray for be guided along a high index core, its incident angle must surpass both materials' critical angles. Otherwise, a portion of the ray will be transmitted to the lower index medium. We call this region in the dispersion relation with forbidden propagation the light-cone, where a continuous spectrum of radiating plane waves exists rather than a discrete spectrum. This discreteness of solutions is a general property is a general property of boundary value problems (this will be expanded in the following chapter).

While the previous analysis provided insightful information about the quantitative behaviour of slab waveguides, it is only valid for a 1 dimensional waveguide. In practical devices, waveguides exist as 3 dimensional structures. While they are mode complex to analyze, the general principles previously established nevertheless hold true. As an example, ridge waveguides can be fabricated by etching a layer of silicon above

a substrate of silicon dioxide. In photonic circuits, those waveguides are integrated with other devices such as Mach-Zender interferometers, couplers, and resonators (the subject of the following section) to process optical signals. Another example of technological important is the optical fiber, where a cylindrical cable of dielectric layers is used to transmit unprecedented data bandwidth for telecommunication applications.
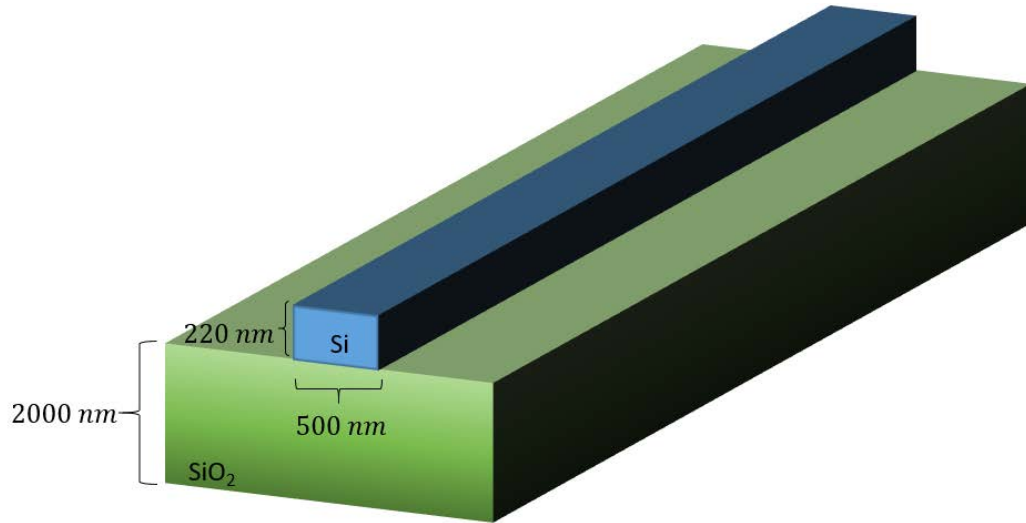
Figure 6: A typical design of a silicon ridge waveguide. The silicon device is deposited on top of a silicon dioxide substrate. The geometrical features correspond to a design allowing only the fundamental mode to exist.

2.3 Dielectric optical resonators

We will now shift our focus to another class of optical devices, the dielectric resonators. Whereas waveguides are able to guide electromagnetic energy along a propagation direction, optical resonators confine energy in space. In both cases, this confinement can be achieved by the appropriate geometry and material boundary. By only allowing a discrete set of resonant frequencies, resonators can act as 'filters' for light. We will begin by consider universal properties and applications of optical resonators, and we will then examine in more detail a particularly important class of resonators: the whispering-gallery modes (in particular, the microring).

2.3.1 Attributes of optical resonators

Just as with optical waveguides, in order to study the general features of dielectric resonators, our starting point is with Maxwell's wave equations [14]. However, we will now only assume oscillation in time, where the field amplitude is modulated by a complex exponential of a single frequency, which may be complex when we consider dissipation of energy. In general, resonators are able to supports multiple modes, which form a complete orthonormal basis. By providing appropriate boundary conditions (along with a suitable coordinate system [15], depending on the resonator's geometry), we are able to solve for the allowed fields and resonant frequencies. In other words, the real part of our electric field for multiple modes takes the general form:

$$E(t) = \sum_{i=1}^{n} A_n \cos(w_n t) e^{-bt} \tag{19}$$

With b being a constant responsible for the various loss mechanism. We can obtain more information about a particular set of resonant modes by analyzing the electric field's signal in the frequency domain, where we take the Fourier transform of the sum of damped oscillators. By doing so, we obtain a sum of Loretzians, written as:

$$E(\omega) = \sum_{i=1}^{n} \frac{A_n}{(\omega_n - a)^2 + b^2} \tag{20}$$

In the frequency domain, we are able to more easily visualize the resonances. From the loss parameter b, as it increases, the resonances decay faster in the domain, while in the frequency domain, the full width half maximum (or its linewidth) decreases. Clearly, in order to have low loss resonators, its resonances must be made to be sharp. In this case, the electric field amplitude will be made to be very high. A universal measure of optical losses in resonators is its quality factor, which is proportional to how long electromagnetic energy can be stored. The Q-factor can be written as:

$$Q = \frac{\lambda}{FWHM} \tag{21}$$

For various applications, it may be desirable to have high Q-factor modes. In sensing, for example, narrower resonances make it easier to detect shifts, which is critical for

fabricating high sensitivity sensors [16].

We may also refer to the distances between 2 adjacent resonances. The free spectral range (FSR) can thus be expressed as:

$$FSR = \lambda_m - \lambda_{m-1} \tag{22}$$

One interesting case of 2 adjacent resonances always being equal is the microring, whose resonance condition depend on an integer number of wavelengths fitting in its circumference.

For more complex cavities, it may be difficult, or impossible, to calculate the fields and resonant wavelengths. Furthermore, in realistic situations, there may be imperfections along the surface, making an exact analytic calculation intractable. By using an approach from perturbation theory, we can treat imperfections as having only a small effect on the solution. We can then construct an approximate answer by starting with the solution to the known, unperturbed case. By adding a small contribution in $\Delta\varepsilon(\mathbf{r})$ and $\Delta\mu(\mathbf{r})$ to the dielectric function and assuming that the perturbed and unperturbed fields are equal, the shift in resonance frequency from a perturbation can be approximated as:

$$\frac{\omega - \omega_0}{\omega} \approx -\frac{\int_{\Delta V} \left[\mathbf{E}^* \varepsilon_0 \Delta\varepsilon(\mathbf{r})\mathbf{E} + \mathbf{B}^* \mu_0 \Delta\mu(\mathbf{r})\mathbf{B} \right] dV}{\int_V \left[\varepsilon_0\varepsilon(\mathbf{r})\mathbf{E}^* \cdot \mathbf{E} + \mu_0\mu(\mathbf{r})\mathbf{B}^* \cdot \mathbf{B} \right] dV}$$

Which is the well-known Bethe-Schwinger cavity perturbation formula [17]. For small enough radiation losses (which is realizable with a large enough resonator and high Q-factor, thus only a minimal amount light will leak out), we can integrate over the volume of the resonator.

There are three broad categories of resonators:

1. **Fabry-Perot cavities:** The simplest geometry, it consists of 2 parallel mirrors, where light can continuously be reflected [18]. Resonance occurs when the distance between the mirrors is an integer multiple of the operating wavelength. Their main purpose is to construct laser cavities, whereas their difficulty to be integrated limits their usefulness in photonic circuits.

2. **Whispering-gallery modes:** As discovered by Lord Rayleigh waves are able to travel along the circumference of a curved surface by total internal reflection and repeatedly striking the surface as it propagates. In photonics, this has been realized with the toroid, ring, disk, and microbottle geometries [19]. These resonators have the potential to reach Q-factors of up to 10^9, as their losses can be mitigated by fabricating larger diameters (to maximize total internal reflection).

3. **Photonic crystal cavities:** In periodic dielectric structures (which will be explored in detail next chapter), there may exist bandgaps; frequency ranges where propagation is forbidden, even while being under the light cone. By creating a defect (for instance, by reducing in size or shifting a unit cell), we can create a localized state for light within the bandgap to be trapped. These cavities can be made to have some of the lowest modal volumes available [20].

2.3.2 Optical ring resonators

We will now introduce an important type of resonator used in photonics: the ring resonator [21]. By looping a straight waveguide onto itself, we can create a structure where light travels multiple circuits around. Just as with the waveguide, the ring resonator uses the concept of total internal reflection to confine the light. While in principle, true total internal reflection can only occur for perfectly straight surfaces, by having a large enough radius such that $R > \lambda$,

In order for a resonance to occur in a ring structure, the wave travelling in the loop must constructively interfere with itself. Otherwise, for destructive interference, the field will greatly decrease. At the resonance condition, for particular wavelengths, λ_m, a high buildup of energy will occur. In order to have a resonance, an integer number of wavelengths must fit around the circumference of the ring. This condition can be expressed as:

$$\lambda_m m = 2\pi n_{\text{eff.}} R$$

With m representing the mode number and $n_{\text{eff.}}$ being the mode's effective index. This implies that the spectrum of a ring resonator has peaks at these resonant wavelengths
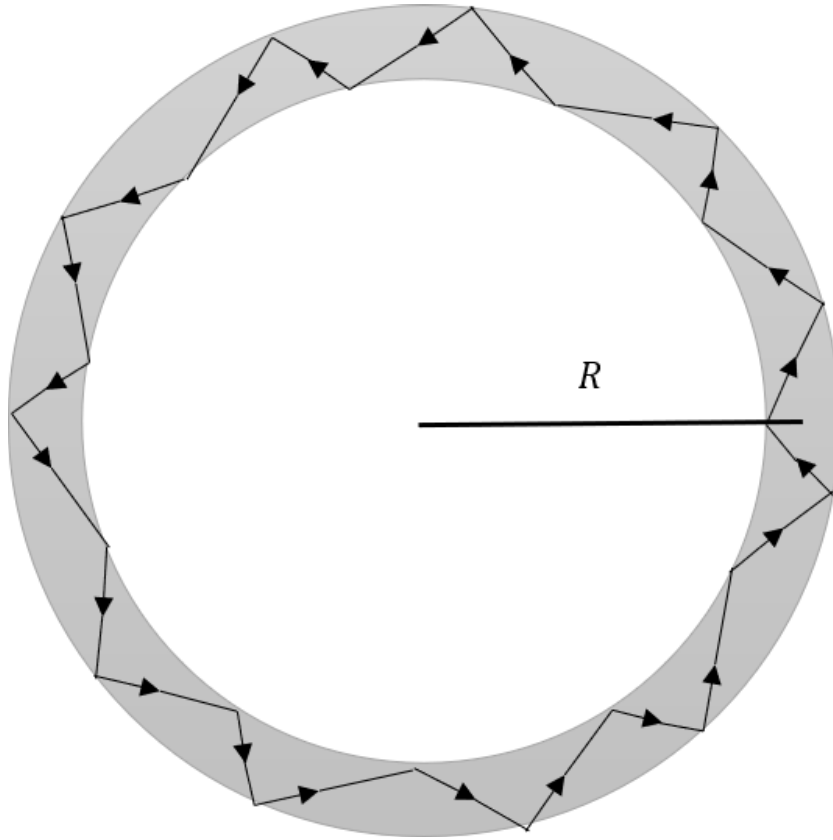
Figure 7: An optical ray being continuously reflected along the perimeter of an optical ring resonator, showing an example of a whispering gallery mode.

that are equally spaced apart. In other words, the free spectral between all adjacent resonances is constant.

There are three main sources of optical losses in ring resonators and waveguides:

1. **Absorption from materials:**   This can occur from electronic processes in the semiconductor materials, such as molecular vibrations, free carrier absorption, and interband transitions [22]. Even when far away from transition, there is always residual absorption.

2. **Electromagnetic scattering:**   During the fabrication of process, small contaminants imperfections appear on the dielectric surface. As the wave experiences small defects, some light will inevitably be scattered out of the device. On the sidewalls, the surface roughness can be several nanometers, having a detrimental effect on the performance of waveguides.

3. **Radiation losses:** Leakage arises for particular waveguide and resonator geometries when the fields are not true solutions to the wave equations. Physically, this typically manifests itself as bending loss, or leakage to the cladding/substrate. Bending loss occurs when the bending radius is small, the conditions of total internal reflection cannot be met. Leakage to the substrate or cladding occurs due to the contrast in index of refraction. For a low enough contrast, the evanescent field at the interface will extend further, causing optical losses.

2.4 Coupled mode theory

When two waveguides or resonators are brought to close proximity (such that their evanescent fields overlap), a mutual exchange of energy occurs. This section will consider the coupling of optical in both space and time by developing a general formalism, starting from the basic postulates. In the literature, there have been multiple approach to the problem of modal coupling, including perturbation theory [23], a variational approach [24], and reciprocity of fields and dielectric functions [25]. We will develop the formalism of 2 coupled resonators in time to show mode splitting.

Let us first consider 2 lossless resonators with amplitudes a_1 and a_2. Uncoupled, their differential equations can be written as:

$$\begin{aligned} \frac{da_1}{dt} &= i\omega_1 a_1 \\ \frac{da_2}{dt} &= i\omega_2 a_2 \end{aligned} \tag{23}$$

By coupling them (for instance, bringing them close to each other), we change their time dependence and introduce coupling coefficients, κ_{12} and κ_{21} . In the limit of weak coupling,

$$\begin{aligned} \frac{da_1}{dt} &= j\omega_1 a_1 + j\kappa_{12} a_2 \\ \frac{da_2}{dt} &= j\omega_2 a_2 + j\kappa_{21} a_1 \end{aligned} \tag{24}$$

In the weak coupling regime, their time dependences are only weakly perturbed by introducing coupling coefficients. In this regime, the new terms are only important when $\omega_1 \approx \omega_2$. For orthogonal modes, even when coupled, energy must be conserved,

and can be written as its sum of the amplitudes, $W = |a_1|^2 + |a_2|^2$. For lossless coupling, we can rewrite the differential equation as:

$$\frac{d}{dt}\left(|a_1|^2 + |a_2|^2\right) = j\kappa_{12}a_1^*a_2 + j\kappa_{21}a_2^*a_1 - j\kappa_{12}^*a_1a_2^* - j\kappa_{21}^*a_2a_1^* = 0 \qquad (25)$$

Which can only be obeyed by the constraint on the coupling coefficient (which is true for lossless coupling):

$$\kappa_{12} = \kappa_{21}^* = \kappa. \qquad (26)$$

By introducing the above condition in the two initial differential equations and assuming a general time dependence of the form $\exp(i\omega t)$, we are able to solve for the two roots of the frequency to obtain:

$$\omega = \frac{\omega_1 + \omega_2}{2} \pm \sqrt{\left(\frac{\omega_1 - \omega_2}{2}\right)^2 + |\kappa|^2} \qquad (27)$$

We now have two real frequencies, corresponding to modes whose energies are conserved. This result implies that resonant modes can be split. This is a known phenomenon from quantum mechanics, where a degenerate energy level in a perturbed system can result in a splitting of the eigenvalues, such as in the Stark and Zeeman effects. If at $t = 0$, only one resonator is excited and they both the same resonant frequency, the excitation will 'bounce' back and forth. For two resonators that do not support the same resonant frequencies, the energy transfer is not complete.

Chapter 3

Optics in periodic structures

The theory of quantum condensed matter has explained many phenomena about the electronic properties of crystals (a periodic arrangement of electron sites). For example, it explains how a material can behave like an electrical insulator or conductor. The crystal's periodic potential and geometry dictates those properties, from which the Schrodinger equation can be used to solve for the dynamics of a propagating electron.

As both electron and photons obey wave equations (Schrodinger's and Maxwell's), this chapter will explore some of the properties of periodic arrangements of dielectric functions, similar to the electron in a periodic potentials. In optics, the analogue of electronic crystals are photonic crystals, which provide another mean to control optical modes.

3.1 Electromagnetic eigenvalue problems

In quantum mechanics, the Schrodinger equation for an electron experiencing a potential V can be written as the following [26]:

$$\left(-\frac{\hbar^2}{2m}\nabla^2 + V(\mathbf{r}) \right) \Psi = E\Psi \tag{28}$$

$$H\Psi = E\Psi \tag{29}$$

For an electron in a periodic potential, it must repeat itself for every unit cell. By letting $\mathbf{R}$ be the lattice vector of our crystal, which dictates the distances between the potential sites, any general periodic potential is expressed as:

$$V(\mathbf{r} + \mathbf{R}) = V(\mathbf{r}) \tag{30}$$

This implies that the electron's wavefunction is also periodic. The statement of Bloch's theorem gives us a general form of the wavefunction: a plane wave modulated by an envelope function which depends upon the periodic potential [27]. The statement of Bloch's theorem is as follows:

$$\Psi(\mathbf{r}) = e^{i(\mathbf{k}r)}u(\mathbf{r}) \tag{31}$$

Thus, by substituting this general form of the wavefunction in Schrodinger's equation, our new problem is now to find $u(\mathbf{r})$. This new quantity is also periodic, so we also have $u(\mathbf{r} + \mathbf{R}) = u(\mathbf{r})$.

In photonics, we instead consider an electromagnetic wave propagating through a medium with a particular dielectric function, $\epsilon(\mathbf{r})$. Similarly to condensed matter physics, our dielectric function can be constructed as to be periodic (for example, by repeating a pattern of dielectric rods). Similarly to the periodic potential, our periodic dielectric function is written as:

$$\epsilon(\mathbf{r}) = \epsilon(\mathbf{r} + \mathbf{a}) \tag{32}$$

Similarly to electrons, where the potential's strength dictates whether the material is a conductor insulator, photonic bandgaps can open if the contrast in dielectric function is high enough. Indeed, photonic crystals can be designed as to prevent propagation of electromagnetic waves in a range of frequencies.

As previously treated for waveguides and resonators, we can consider a single mode of electromagnetic wave (similarly to quantum mechanics, where for a time-independent potential, we can modulate the wavefunction by a plane wave of a single energy):
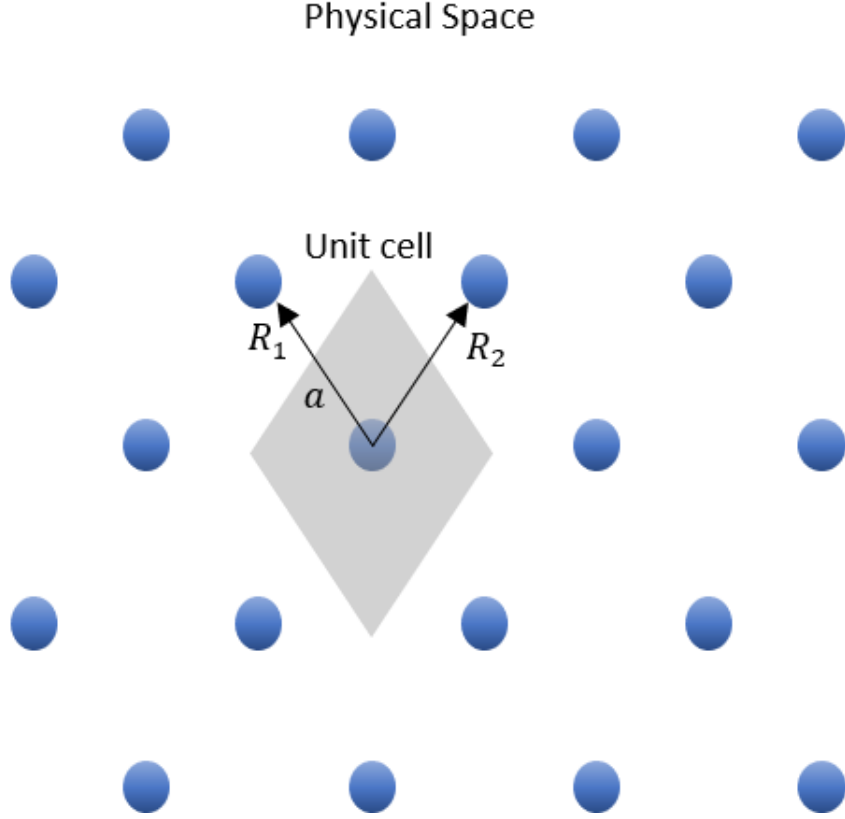
Figure 8: A periodic arrangement of dielectric rods in a hexagonal lattice. The lattice vectors $\mathbf{R_1}$ and $\mathbf{R_2}$ are shown, and the basic unit cell of the lattice is denoted by the shaded region.

$$
\begin{aligned}
\mathbf{B}(\mathbf{r}, t) &= \mathbf{B}(\mathbf{r})e^{-i\omega t} \\
\mathbf{E}(\mathbf{r}, t) &= \mathbf{E}(\mathbf{r})e^{-i\omega t}
\end{aligned}
\tag{33}
$$

These can be put in the two curl equation for the fields. In the frequency domain, the time derivatives now become imaginary frequency terms. As such, the (not yet uncoupled) equations now become:

$$
\begin{aligned}
\nabla \times \mathbf{E}(\mathbf{r}) - i\omega\mu_0\mathbf{B}(\mathbf{r}) &= 0 \\
\nabla \times \mathbf{B}(\mathbf{r}) + i\omega\varepsilon_0\varepsilon(\mathbf{r})\mathbf{E}(\mathbf{r}) &= 0
\end{aligned}
\tag{34}
$$

As previously done, we can uncouple the equations by taking the curl of both equations and using a vector identity to remove the divergence terms (will follows from Gauss's laws). This results in:

$$\nabla \times \left(\frac{1}{\varepsilon(\mathbf{r})}\nabla \times \mathbf{B}(\mathbf{r})\right) = \left(\frac{\omega}{c}\right)^2 \mathbf{B}(\mathbf{r})$$
$$\nabla \times (\mu_0 \nabla \times \mathbf{E}(\mathbf{r})) = \left(\frac{\omega}{c}\right)^2 \mathbf{E}(\mathbf{r}) \tag{35}$$

This is the so-called master equation for optics [28]. Together with the tranversality (Gauss's laws) of the fields and a dielectric function, we are able to find any information about our electromagnetic fields.

To apply periodicity to our field functions, just as with the quantum wavefunction, we can apply Bloch's theorem to the spatial component, giving us:

$$\mathbf{B}(\mathbf{r}) = e^{(i\mathbf{k}\cdot\mathbf{r})}\mathbf{u_k}(\mathbf{r})$$
$$\mathbf{E}(\mathbf{r}) = e^{(i\mathbf{k}\cdot\mathbf{r})}\mathbf{w_k}(\mathbf{r}) \tag{36}$$

With being $\mathbf{u}(\mathbf{r})$ and $\mathbf{w}(\mathbf{r})$ being the periodic functions to be solved from the photonic crystal's dielectric function.

For the most complete general solution of the fields, we can combine Bloch's theorem and the time dependence to obtain the following expression for the fields:

$$\mathbf{B_k}(\mathbf{r},t) = \mathbf{u_k}(\mathbf{r})e^{(i\mathbf{k}\cdot\mathbf{r}-\omega t)}$$
$$\mathbf{E_k}(\mathbf{r},t) = \mathbf{w_k}(\mathbf{r})e^{(i\mathbf{k}\cdot\mathbf{r}-\omega t)} \tag{37}$$

In the master equation, a linear differential operator is applied to the fields, and if there is indeed a permitted function which satisfies a particular problem, then it returns a constant multiplied by the field itself. This situation occurs frequently in the physics of waves, and is an eigenvalue problem.

By borrowing the language of linear algebra, by taking parallels, the curl-curl operator acting on the field is the linear operator, the field is the eigenvector, and the allowed frequencies are the eigenvalues. We can rewrite the master equation more succinctly to make the analogy more transparent:

$$\Theta\mathbf{B}(\mathbf{r}) = \left(\frac{\omega}{c}\right)^2 \mathbf{B}(\mathbf{r})$$
$$\Theta\mathbf{E}(\mathbf{r}) = \left(\frac{\omega}{c}\right)^2 \mathbf{E}(\mathbf{r}) \tag{38}$$

With Θ acting as the linear differential operator. We can immediately see the similarity to $\mathbf{A}f = \lambda f$ [29].

Every solution of the eigenvalue problem of a photonic crystal consists of its spectrum of discrete modes. The profile of this spectrum depends on the spatial domain of the fields. Specifically, if the fields are bounded in space by some boundary conditions, whether bounded by a geometry or by imposing periodicity, then these frequencies will form a discrete set, which can be seen by observing the dispersion relation. This qualitative feature is also seen in waveguides and resonators, where only a finite number of propagating modes/resonant frequencies are permitted by the system. Otherwise, for radiating waves (such as those found beyond the light cone of a waveguide), the frequencies form a continuous range. This is a general property of Hermitian eigenvalue problems in physics which can be argued to originate from the orthogonality of the modes.

3.2 Reciprocal space

By using Bloch's theorem, we can express an electromagnetic mode as a function (whose periodicity matches that of the crystal's) modulated by a plane wave. It can be argued that we only need to have the mode's wave vectors, $\mathbf{k}$, in a particular region to obtain all necessary physical information about the photonic crystal.

For a function that is periodic on lattice (in our case, the dielectric function or potential), such that $\epsilon(\mathbf{r} + \mathbf{R})$ is true for all vectors $\mathbf{R}$ which connects one lattice points to another, or translates the lattice.

For any periodic function, it can be constructed out of plane waves of various wave vectors by the Fourier transform. For a smooth function f, its Fourier transform can be written as:

$$f(\mathbf{r}) = \int d^3\mathbf{q}\, g(\mathbf{q}) e^{i\mathbf{q}\cdot\mathbf{r}} \tag{39}$$

With $g(\mathbf{q})$ being a plane wave's coefficient. As our dielectric function is periodic on a lattice, this requires $f(\mathbf{r} + \mathbf{R})$. The vectors $\mathbf{q}$ are also called reciprocal lattice vectors, and they themselves also form a lattice of their own.

From a set of lattice vectors in physical space, they can be converted to an associated set of reciprocal lattice vectors. If we let $\mathbf{R} = \mathbf{a_1}, \mathbf{a_2}, \mathbf{a_3}$, be the lattice vectors in physical space, and exploit features of the cross-product, their associated reciprocal lattice vectors as be written as:

$$\mathbf{b}_1 = \frac{2\pi \mathbf{a}_2 \times \mathbf{a}_3}{\mathbf{a}_1 \cdot (\mathbf{a}_2 \times \mathbf{a}_3)}, \quad \mathbf{b}_2 = \frac{2\pi \mathbf{a}_3 \times \mathbf{a}_1}{\mathbf{a}_1 \cdot (\mathbf{a}_2 \times \mathbf{a}_3)}, \quad \mathbf{b}_3 = \frac{2\pi \mathbf{a}_1 \times \mathbf{a}_2}{\mathbf{a}_1 \cdot (\mathbf{a}_2 \times \mathbf{a}_3)} \tag{40}$$

This means that if we take the Fourier transform of a function on a periodic lattice, only terms with wave vectors that are reciprocal space vectors are physically meaningful.

Previously, we explained that a discrete electromagnetic mode can be written as a periodic function modulated by a plane wave. As this function shares the periodicity of the lattice, this means:

$$\mathbf{E_k}(\mathbf{r}) = e^{i\mathbf{k} \cdot \mathbf{r}} \mathbf{u_k}(\mathbf{r} + \mathbf{R}) = e^{i\mathbf{k} \cdot \mathbf{r}} \mathbf{u_k}(\mathbf{r}) \tag{41}$$

As per the periodicity, these Bloch modes with different values of the wave vectors $\mathbf{k}$ need not result in different modes. In particular, we can add reciprocal lattice vectors to a wave vector and periodicity will still apply. Due to this redundancy, we can restrict ourselves to a particular region, also called the (usually focusing on the first) Brillouin zone. Graphically, this can be represented by taking all of the volume of a unit cell that is the closest to a particular lattice point compared to any other.

This fact can be exploited to make calculations of photonic crystals much easier. Instead of sweeping across all of k-space, we can instead only consider the points of high symmetry of the unit cell, corresponding to the corners of the first Brillouin zone. In k-space, if we replace the fields with the general form of Bloch's theorem, we get:

$$(i\mathbf{k} + \nabla) \times \frac{1}{\varepsilon(\mathbf{r})} (i\mathbf{k} + \nabla) \times \mathbf{u_k}(\mathbf{r}) = (\omega(\mathbf{k})/c)^2 \mathbf{u_k}(\mathbf{r}) \tag{42}$$

Now, our original eigenvalue problem for the electromagnetic mods are merely restricted to a single unit cell of the lattice, in k-space. As $\mathbf{k}$ is now made to vary continuously, for a given integer n (which arises from the system's boundary conditions,
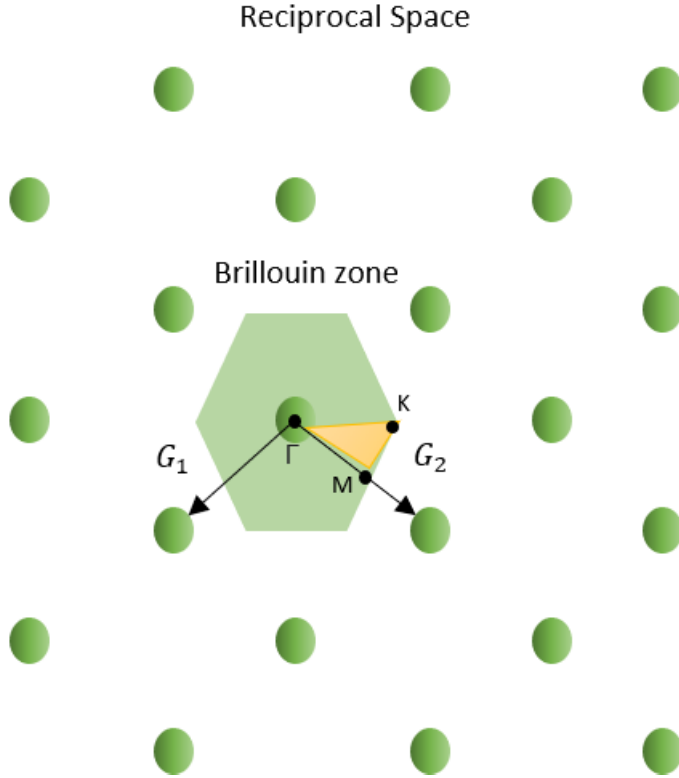
Figure 9: The reciprocal lattice space of the hexagonal lattice. The reciprocal lattice vectors are denoted by $\mathbf{G_1}$ and $\mathbf{G_2}$, and the first Brillouin zone is indicated in the yellow shaded region.

as discussed with waveguides. The dispersion relation is thus composed of discrete $\omega_n(\mathbf{k})$ (also called bands), which can have band gaps depending on the strength of the dielectric contrast of the perturbation.

In practice, to calculate the dispersion relation of a given lattice and $\epsilon(\mathbf{r})$, numerical techniques are used, such as eigenvalue solvers and a plane wave expansion methods. These techniques will be briefly outlined in appendix b.

A simple and important system which illustrates these concepts is the one dimensional photonic crystal (such as an infinite set of planes, or a periodic perturbation to a waveguide). For a lattice vector $\mathbf{a} = a\hat{x}$, with a being the length of the unit cell, $\mathbf{b} = \frac{2\pi}{a}\hat{x}$. This fact can be used to find the dispersion relation of a linear waveguide, resulting in an equivalent formulation to the previously outlined boundary value problem approach. A periodic perturbation can also be applied to a waveguide to open a bandgap.

3.3 Comparison with quantum mechanics

Throughout the chapter, we have made references to properties of optics in periodic dielectric functions which are mathematically analogous to quantum condensed matter. Indeed, both fields study the propagation of waves (whether physical or abstract) in a periodic medium, so the mathematical structure of the eigenvalue problems bear many similarities. However, there are also some physical differences.

One different of practical importance is that in quantum mechanics, for potentials being separable by a sum $V(\mathbf{r}) = V_x(x) + V_y(y) + V_z(z)$, we can rewrite the wavefunction as a function of products $\Psi(\mathbf{r}) = X(x)Y(y)Z(z)$. From this, it allows for Schrodinger's equation to be solved by the method of separation of variables. In electromagnetism, however, this kind of factorization is generally not possible due to the curl of the hermitian operator, which couples different spatial components together. Typically, one resorts to numerical methods to solve for the eigenmodes of a photonic crystal.

This following table aims to summarize the main parallels and difference between the eigenmodes in a periodic quantum system and in a photonic crystal. These analogies will be important in the topic of topology in optical systems.

	Quantum mechanics	Electromagnetism
Field	$\Psi(\mathbf{r}, t) = \Psi(\mathbf{r})e^{-iEt/\hbar}$	$\mathbf{B}(\mathbf{r}, t) = \mathbf{B}(\mathbf{r})e^{-i\omega t}$
Hermitian operator	$\hat{H} = -\frac{\hbar^2}{2m}\nabla^2 + V(\mathbf{r})$	$\hat{\Theta} = \nabla \times \frac{1}{\varepsilon(\mathbf{r})}\nabla \times$
Eigenvalue equation	$\left[-\frac{\hbar^2}{2m}\nabla^2 + V(\mathbf{r})\right]\Psi_E(\mathbf{r}) = E\Psi_E(\mathbf{r})$	$\nabla \times \frac{1}{\varepsilon(\mathbf{r})}\nabla \times \mathbf{B}(\mathbf{r}) = \frac{\omega^2}{c^2}\mathbf{B}(\mathbf{r})$
Bloch's theorem	$\psi_{n,\mathbf{k}}(\mathbf{r}) = e^{i\mathbf{k}\cdot\mathbf{r}}u_{n,\mathbf{k}}(\mathbf{r})$	$\mathbf{B}_{\mathbf{k}}(\mathbf{r}) = \mathbf{u}_{\mathbf{k}}(\mathbf{r})e^{i\mathbf{k}\cdot\mathbf{r}}$
Condition on field function	$\int_{-\infty}^{+\infty}|\Psi(x,t)|^2\,\mathrm{d}x = 1$	Fields must obey Gauss's laws $\nabla \cdot \mathbf{B} = 0$
Periodicity of the system	$V(\mathbf{r}) = V(\mathbf{r}+\mathbf{R})$, with the lattice vectors $\mathbf{R}$	$\varepsilon(\mathbf{r}) = \varepsilon(\mathbf{r}+\mathbf{R})$, with the lattice vectors $\mathbf{R}$
Bands of the dispersion relation	$E_n(\mathbf{k})$ for the energies of the eigenstates	$\omega_n(\mathbf{k})$ for the frequencies of the harmonic modes
Length scale	Set by physical constants	Solutions are scale-free

Table 1: The mathematical and physical similarities between quantum condensed matter and electromagnetism in a periodic medium.

Chapter 4

Topology in physics

As previously outlined, the mathematical analogies between condensed matter and optics in periodic systems are rich. This lets us exploit the geometry to design and control the behaviour of light in novel ways.

The concept of topology in mathematics concerns itself with shapes that can be deformed continuously into other shapes. The field of condensed matter draws inspiration from the discovery of the quantum Hall effect and topological insulators, which enables robust, unidirectional propagation of current. Due to the correspondence between Schrodinger's and Maxwell's equations, we are able to study these concepts in an optical context, which has opened the field of topological photonics. We will begin by developing the theory of topology in quantum condensed matter, due to it being a more developed theory before exploring these properties in photonics. This chapter will introduce the basic concepts of topology in condensed matter, and we will then discuss models that have been implemented in optics, including the Su-Schrieffer-Heeger model.

4.1 Topological invariants

In mathematics, shapes of the same general classification which can be smoothly deformed into one another is the subject of topology. Instead of classical geometry, which concerns itself with the specific structure of a geometrical entity, topology aims to describe the global structure.

As an example, in the figure below, a sphere can be continuously deformed into a wine glass without creating a hole. As such, both the sphere and wine glass are said to have the same topological invariant, characterized by the number of holes. But, a sphere cannot be deformed smoothly into a torus or a mug without making a hole, meaning their topological invariant is different. In order to change this topological invariant into another one, it must go through a topological phase transition.
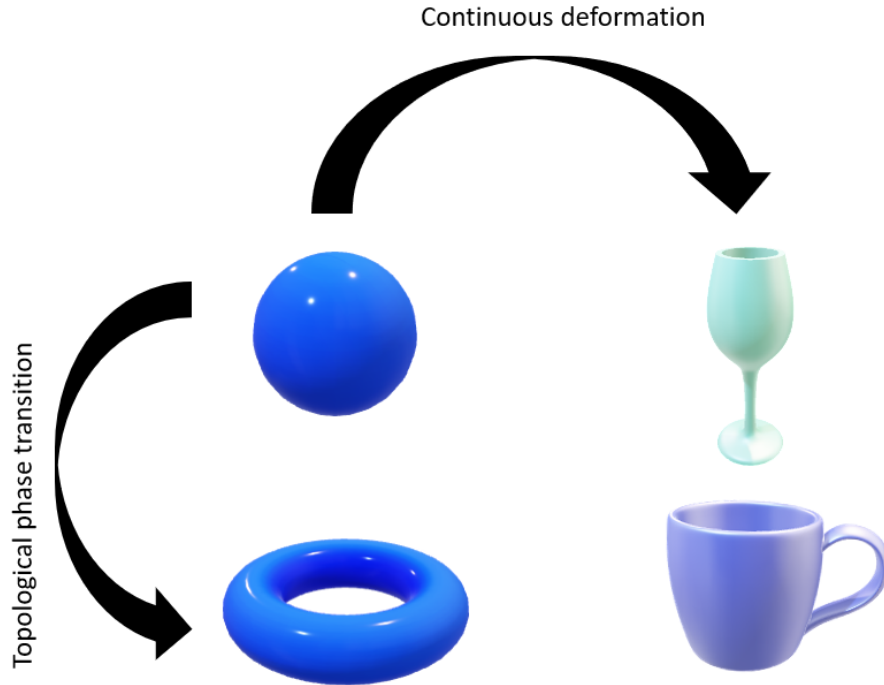
Figure 10: Shapes with the same amount of holes may be continuously deformed into each other and said to have the same topological invariant. When a hole is closed or formed, a topological phase transition occurs (from example, from a sphere to a torus).

This property has profound physical consequences in the study of condensed matter systems [30]. Instead of considering geometric volume, we can instead classify a system's Hamiltonian as such. A particle in a state separated from another cannot be deformed into it without experiencing a bandgap. In direct analogy with the purely geometrical case, a hole created by a topological phase transition is analogous to crossing a bandgap from one state to another.

First hints of topology concepts in physics arose when the quantum Hall effect was first studied [31]. Here, a two-dimensional gas of electrons is in the presence of a

perpendicular magnetic field. What was found was the conductance being quantized at robust plateaus, at integer values times $e^2/\hbar$. This integer is related to a system's topological invariant, a quantity that describes the global structure of a particle's state in the Brillouin zone.

As before, to handle a particle's state in a periodic lattice, we can invoke Bloch's theorem by using a function whose periodicity matches that of the crystal's:

$$\psi_{n,\mathbf{k}}(\mathbf{r}) = e^{i\mathbf{k}\cdot\mathbf{r}}u_{n,\mathbf{k}}(\mathbf{r}) \tag{43}$$

With n indicating the n-band of the dispersion relation. This wavefunction naturally obeys the Schrodinger eigenvalue equation in k-space as such:

$$\hat{H}_{\mathbf{k}}u_{n,\mathbf{k}}(\mathbf{r}) = E_n(\mathbf{k})u_{n,\mathbf{k}}(\mathbf{r}) \tag{44}$$

The properties of a band can in part be captured by its global geometric properties and how it varies continuously with the wave vector. This geometry can be explained by an eigenstate's Berry phase [32]. More specifically, we will restrict ourselves to values of the wave vector $\mathbf{k}$ which only spans the first Brillouin zone. Qualitatively, we can think of a particle moving from a state in band n and make it adiabatically move along this band in a closed path. By moving in k-space, this particle will now have a phase, which we denote by the Berry phase:

$$\gamma = \oint \mathcal{A}_n(\mathbf{k}) \cdot d\mathbf{k} \tag{45}$$

The quantity $\mathcal{A}_n(\mathbf{k})$ is defined as the Berry connection:

$$\mathcal{A}_n(\mathbf{k}) = i\left\langle u_{n,\mathbf{k}} \left| \nabla_{\mathbf{k}} \right| u_{n,\mathbf{k}} \right\rangle$$

To fully encode the geometry of the nth band, we can construct a gauge invariant Berry curvature:

$$\Omega_n(\mathbf{k}) = \nabla_{\mathbf{k}} \times \mathcal{A}_n(\mathbf{k}) \tag{47}$$

However, although the Berry curvature can be continuously defined over ther first Brillouin zone, the phase of the wavefunction is in general not continuous. To determine whether or not this phase is continuous depends on the particular topological invariant of the band. From the Berry curvature, we can calculate a particular topological invariant, the Chern number from this integral:

$$C_\mathrm{n} = \frac{1}{2\pi} \int_\mathrm{BZ} d^2k \Omega_n \left(k_x, k_y, k_z\right) \tag{48}$$

Overall, this Chern number is zero if the Berry connection can be defined continuously over the Brillouin zone, by Stokes theorem. Otherwise, with a non-zero Chern number, it implies that the particle's state cannot be defined continuously. The Chern number is always an integer value. One consequence of the Chern number is that its value remains invariant under perturbations, as long as a bandgap (which separates states from being continuously deformed into each other otherwise) remains open. Systems with this property are also called topological insulators. To distinguish states with different topological invariants, we say that a state with a Chern number of 0 is topologically trivial, otherwise it is topological.

For one-dimensional Hamiltonians with chiral symmetry (where the sign of the spatial coordinate remains invariant under sign inversion), there exists a simpler way to classify and calculate its topological invariant. Those Hamiltonians, when Fourier transformed to k-space, a more generic form may be adopted:

$$\hat{H}(k) = \begin{pmatrix} \mathbf{0} & Q(k)^\dagger \\ Q(k) & 0 \end{pmatrix} \tag{49}$$

With $Q(k)$ being an n x n matrix for a unit cell with $2n$ possible sites, which satisfies the periodicity of the lattice. If a gap opens around the zero energy point, the topological invariant can instead be described by its winding number, described by the phase $Q(k) \equiv |detQ(k)|e^{i\theta(k)}$. This winding number takes the form [33]:

$$\mathcal{W} = \frac{1}{2\pi} \int_0^{2\pi/a} dk \frac{d\theta(k)}{dk} \tag{50}$$

Qualitatively, we can think of the winding number as how many times $detQ(k)$ loops around the origin in the complex plane of k-space as k is made to vary along a path

in the Brillouin zone. Like the Chern number, it too can only be made an integer. And, like the Chern number, states with different winding numbers will remain there, even in the presence of perturbations, unless it closes the gap.

An important condition for topology is also illustrated by the winding number: at minimum, we require two states per unit cell in order to have topology, since we can then open a gap. For a single-band system, no gap can exist or open. It can also be shown that the calculated winding number for such a system will always be 0, and as such, topologically trivial.

As a last example of a topological invariant in condensed matter, which is related to the Berry connection and serves as another specific case of the Chern number, is the Zak phase [34].

$$\mathcal{Z} = i \oint dq \, \langle u_q \mid \partial_q u_q \rangle \tag{51}$$

Which is simply, again, the integration of the Berry connection over the first Brillouin zone. It difers by a π factor from the Winding number.

4.2 The SSH model

We will now explore a concrete topological insulator system, the Su-Schrieffer-Heeger (SSH) model, the simplest which illustrates the novel concepts of topological insulators [10].

Consider first a system which consists of a linear chain of atomic sites, separated by hopping coefficient t. By using the second quantization formalism, where the states of particles are represented by creation $\hat{c}_n^\dagger$ and destruction operators $\hat{c}_n$. We use those operators to make particles 'hop' from and to various sites in a lattice. For example, the term $\hat{c}_n^\dagger \hat{c}_{n+1}$ would dictate that the particle state would be switched from n to $n+1$. This formalism is also known as a tight-binding model, which serves as an approximation to study in detail the behaviour of electrons in a crystal as they hop from site to site. The Hamiltonian of an electron hopping in a linear chain can thus be written as:

$$\hat{H} = \sum_{n=1}^{M} \hat{c}_n^\dagger \hat{c}_{n+1} t_n + h.c. \tag{52}$$

Where we use the hermitian conjugate $h.c$ to obtain the full dynamics of all possible hoppings. Such a system has one possible state per unit cell. Its dispersion relation relation can be simply calculated to be:

$$E(k) = cos(ka) \tag{53}$$

Where a is the lattice constant of the chain. Such a system only has one possible band, which means no bandgap can be open. Thus, from the definition of the topological invariant, this system cannot support topological features.

As a simple extension to this system, let us now take instead two sites per unit cell, and shifting them such that the hopping coefficient alternates on a site-per-site basis, where we now have t and t'.

$$\hat{H} = \sum_n \left(t\hat{b}_n^\dagger \hat{a}_n + t'\hat{a}_{n+1}^\dagger \hat{b}_n + \text{h.c.} \right) \tag{54}$$

This is known as the Su-Schrieffer-Heeger model, which represents the simplest one-dimensional topological insulator. By the definition of the winding number, now that we have two sites per unit cell, this model can indeed support a nontrivial topological invariant.

To start, it is required to solve for the eigenstates and energies of this system [35]. We will use the tight-binding formalism, with the Hamiltonian above. We assume a system of infinite extent with periodic boundary conditions to simplify the analysis. As is common in the literature, we can start by taking the discrete lattice Fourier transform of the Hamiltonian, where we replace the second quantization operators as follows:

$$
\begin{aligned}
c_i^\dagger &= \frac{\sqrt{a}}{\sqrt{2\pi}} \int_{\text{BZ}} dk c_k e^{-ikx} \\
c_i &= \frac{\sqrt{a}}{\sqrt{2\pi}} \int_{\text{BZ}} dk c_k e^{ikx}
\end{aligned}
\tag{55}
$$
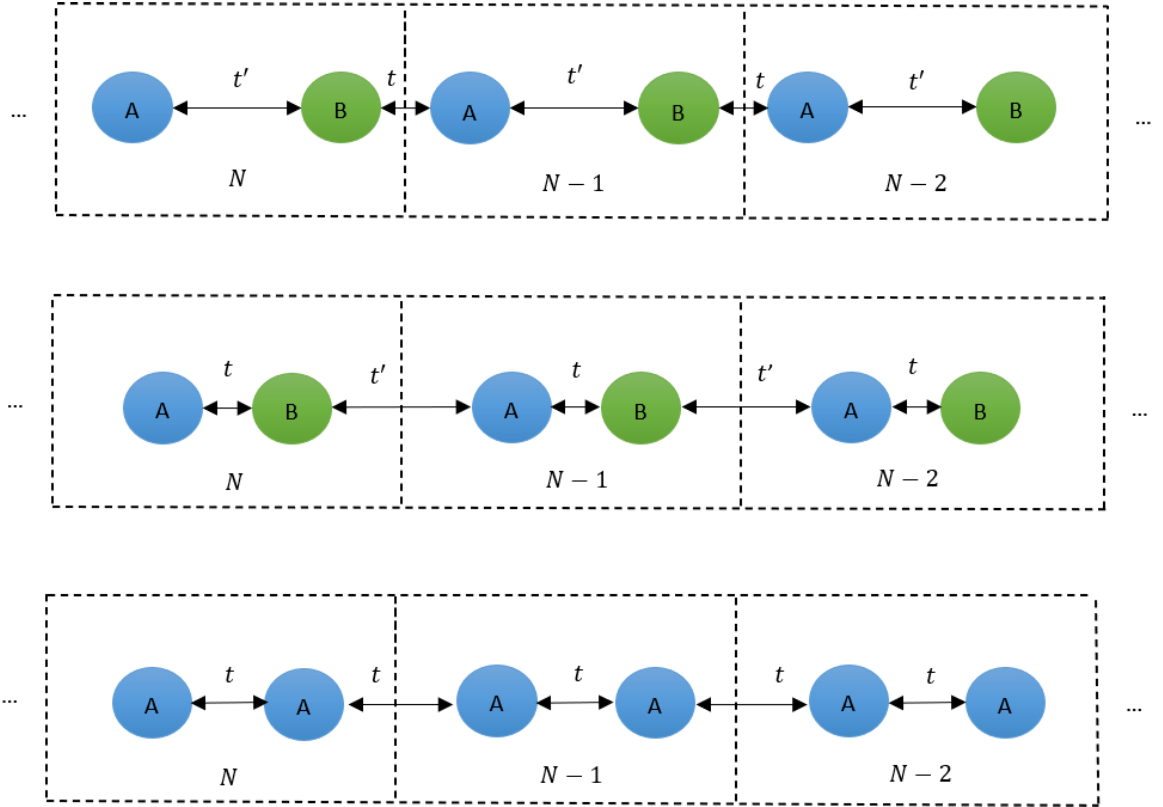
Figure 11: Three different possibilities for the SSH model. The topological configuration when $t' > t$, the trivial configuration when $t > t'$, and the limiting case $t' = t$ are shown in this respective order.

We then replace with the operators of physical space in our Hamiltonian, where we can get the simpler matrix form:

$$\hat{H}(k) = \begin{pmatrix} 0 & t + t'e^{ika} \\ t + t'e^{-ika} & 0 \end{pmatrix} \quad (56)$$

Immediately, we can recognize that it is of the form required by the Winding number, where $Q(k) = t + t'e^{ika}$. Equipped with the Hamiltonian in matrix form, calculating the allowed eigenstates is a simple exercise in linear algebra, where we diagonalize the matrix. Doing so, we obtain an expression :

$$E(k) = \left| t + e^{-ik}t' \right| = \pm\sqrt{t^2 + t'^2 + 2tt'\cos k} \quad (57)$$

As can be seen, this system supports two bands, with a gap opening at around

$E(k) = 0$. When t and t' are equal, it returns to the previous model of a simple chain with one site per unit cell. If this is the case, the gap closes. Otherwise, as the difference in hopping strength $|t - t'|$increases, so does the size of the bandgap. However, the bulk cannot tell the difference in the sign of the difference, so the lattice will appear to be the same. Despite this, the two possibilities will have different topological invariants.
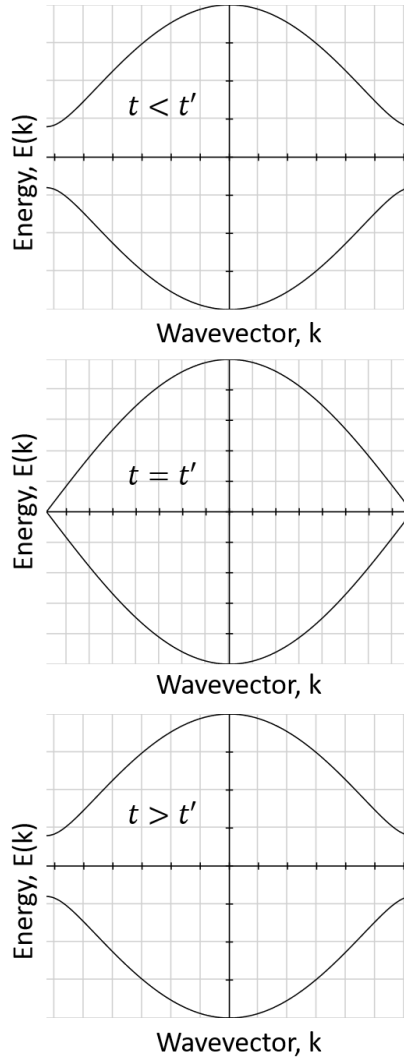
Figure 12: The energy bands of the SSH model. For both the trivial and topological cases, a bandgap is opened by the staggered hopping coefficients, and for gap closes when $t = t'$.

We will now calculate the Zak phases of the SSH model. To start, as we previously identified, the off diagonal function of the Hamiltonian's kernel can be identified

37

as:

$$Q(k) = t + t'e^{-ika} \tag{58}$$

Its phase function is given by:

$$\cot \phi(k) = \frac{t'/t}{\sin ka} + \cot ka \tag{59}$$

Its winding vector can vary across the Brillouin zone for two values of the hopping coefficient's ratio, t'/t. When $t'/t > 1$, the path does not loop around the origin, while if $t'/t < 1$, it does go around the origin and the phase can have any value.

From the Hamiltonian in k-space, we can calculate its eigenvectors, with the phase function $\phi(k)$, to be of the form:

$$|u_k\rangle = \frac{1}{\sqrt{2}} \begin{pmatrix} e^{-i\phi(k)} \\ \pm 1 \end{pmatrix} \tag{60}$$

Then, by using the definition of the Zak phase, we obtain:

$$\mathcal{Z} = \frac{1}{2} \oint dk \frac{d\phi}{dk} = \frac{\Delta\phi}{2} \tag{61}$$

With $\Delta\phi$ representing the path of $\phi(k)$ on the Brillouin zone. The Zak phase is then a π multiple of the Winding number if the path does enclose the origin, or is zero if it does not. So, for both possibilities of dimerization, our topological invariant is:

$$\begin{aligned} \mathcal{Z} = 0 \quad & if \quad t'/t > 1 \\ \mathcal{Z} = \pi \quad & if \quad t'/t < 1 \end{aligned} \tag{62}$$

Again, this means that we can have either a trivial, or topological chain. As such, in order to have a topological phase transition, the bandgap must first be closed (by making both hopping coefficients equal), and then both of the coefficients are reversed from their initial values.

4.3 Topological edge states

Previously, we only only considered the topological properties of systems in their bulk. However, that alone is not sufficient to obtain modes that are robust against perturbations that do not close a bandgap. Another (important) physical interpretation of the topological invariant is the bulk-edge correspondence [36]. As with the quantum hall effect, where the edge current of a sample is robust and unidirectional when surrounded by air (which is topologically trivial), two materials brought together of different topological invariants supports modes (also called topological edge states) that exist in the middle of the bandgap, localized at the interface of the two materials. In a finite sized sample, the edge of the material before air can also support topological edge states.

These edge states can also be said to be protected by symmetry, which are created at an interface by breaking the bulk's symmetry (equivalent to a topological phase transition, or a change in Chern number),

In the literature, there exists a method to classify a Hamiltonian's symmetry based on three different operators. Depending on the permutation of operators that a Hamiltonian satisfies, we can systematically determine if our Hamiltonian can support a topological invariant, . This method is known as the "ten-fold way" [37].

1. **Time-reversal symmetry**: If a Hamiltonian obeys time-reversal symmetry, then it satisfies: $\mathcal{T}H\mathcal{T}^{-1} = H$. Depending on $\mathcal{T}^2$, the Hamiltonian is given a value of 1 for $\mathcal{T}^2 = 1$, or a value of -1 for $\mathcal{T}^2 = -1$ for the ten-fold table. The time reversal operator is defined as: $\mathcal{T} = \gamma \begin{pmatrix} 1 & 0 \\ 0 & 1 \end{pmatrix}$, with γ being the complex conjugation operator.

2. **Chiral symmetry**: The chirality symmetry operator is defined as: $\mathcal{S} = \mathcal{T}\mathcal{C}$, where we sequentially apply both operators to the Hamiltonian. For its value, it can be assigned either a 0 for no chiral symmetry, or 1 for having chiral symmetry. Having chiral symmetry is a requirement for writting the Hamiltonian in matrix form with $h(k)$, which allows to calculate the 1D winding number.

3. **Charge conjugation symmetry**: If a Hamiltonian obeys charge conjugation symmetry, then it satisfies: $\mathcal{C}H\mathcal{C}^{-1} = -H$. Depending on $\mathcal{C}^2$, the Hamiltonian

is given a value of 1 for $\mathcal{C}^2 = 1$, or a value of -1 for $\mathcal{C}^2 = -1$ for the ten-fold table. The form of the charge conjugation operator can be constructed with knowledge of the time-reversal and chirality operators.

By applying those operators to a Hamiltonian and noting the assigned values and the combination, as well as the dimension of the system, we are given a certain "Cartan label", which indicates if we have a topological invariant (0 for being topologically trivial). Thus, if a Hamiltonian supports a topological invariant, it can support topologically protected edge modes.

Cartan label	$\mathcal{T}$	$\mathcal{C}$	$\mathcal{S}$	$d = 0$	$d = 1$	$d = 2$	$d = 3$
A (unitary)	0	0	0	Z	0	Z	0
AI (orthogonal)	+1	0	0	Z	0	0	0
AII (sympectic)	-1	0	0	$2Z_2$	0	Z_2	Z_2
AIII (ch. unit.)	0	0	1	0	Z	0	Z
BDI (ch. orth.)	+1	1	1	Z_2	Z	0	0
CII (ch. sympl.)	-1	-1	1	0	$2Z_2$	0	Z_2
D (BdG)	0	-1	0	Z_2	Z_2	Z	0
C (BdG)	0	-1	0	0	0	$2Z$	0
DIII (BdG)	-1	+1	1	0	Z_2	Z_2	Z
CI (BdG)	+1	-1	1	0	0	0	$2Z$

Table 2: The table for the ten-fold method of classifying topological insulators. By applying the symmetry operators $\mathcal{T}$, $\mathcal{C}$ and $\mathcal{S}$ on the Hamiltonian and noting the system's dimension, we can assign the Hamiltonian a Cartan label, which tells us if it supports a topological invariant.

Going back to the SSH model, we found out that it supports a nontrivial topological invariant by direct calculation, depending on the dimerization parameters. This can indeed be confirmed by the ten-fold way. By applying the three operators and noting the results: time-reversal symmetry gives +1, charge-conjugation gives us 1, and chirality gives 1. By inspection of the table, we can that the Hamiltonian of the SSH model (a one dimensional system) yields the BDI Cartan label, which supports a single topological invariant Z. As such, we can create a topological edge state in the SSH model. To do so, we can take a trivial chain and a topological chain to connect them by a third hopping coefficient, t''. This will guarantee the existence of an edge mode in the middle of both bandgaps.
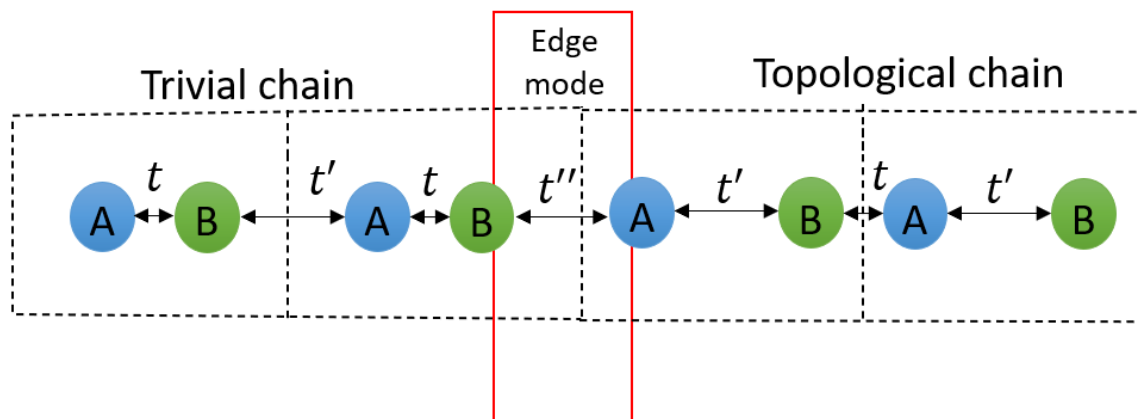
Figure 13: An edge state being implemented in the SSH mode. The edge state exists at the interface between a trivial and topological chain.

4.4 Topological photonics

The study of topology originates from condensed matter systems by the electric current along a sample's edge. An important feature of these systems is that Bloch's theorem holds true, and that the crystal obeys certain symmetries. Since eigenvalue problems in periodic photonic crystals can also be formulated, it should come as no surprise that concepts of topology should also arise in optics [38] [39]. Indeed, a great many systems from condensed matter physics have been constructed by engineering lattices in the optical domain. However, optical systems have features not present in electronic systems.

In electronic systems, its particle obeys Fermionic statistics. In addition, the electrical conductivity is usually measured under weak external fieds, such that the system remains in equilibrium.

However, in optics, since photons are bosons, they obey different statistics, which has an effect at the many-particle level. The quantum statistics of Bosons impose a particular symmetrization requirement on the system's wavefunction under particle exchange. Because of Pauli's exclusion principle, no electrons in the same system can occupy the same quantum state. On the contrary, for the case of weakly interacting bosons at low temperatures, the particles will tend to accumulate in the lowest energy state.

Another process common in optical systems are the nonequilibrium processes that

occur. This manifests itself as, for example, loss mechanisms which reduce the number of photons. This could occur from material absorption, or from the system's geometry, where light is simply radiated away. This alone can have a drastic effect in the ways topological behaviour can exist in these systems.

Instead of breaking time-reversal symmetry by applying a magnetic field to a photonic crystal [40], a simpler experimental setup can be made by realizing topology only by the system's geometry. As a natural analogy to tight-binding models of electrons, the SSH model can be created by making a linear array of resonators with staggered coupling gaps. Thus, the optical modes can be made to couple to different rings, just as electrons can hop between different sites. This system was investigated in the literature for the purpose of using non-Hermiticity to create lasing of the edge mode in this array [41]. In this particular model, the array of rings in the presence of loss and gain possesses $\mathcal{CT}$ symmetry rather than $\mathcal{PT}$ symmetry.

As a possible platform for topological photonics, let us consider a photonic nanobeam cavity, where a linear array of holes along are created along the length of a dielectric beam. To create a cavity in this structure, one can create a trivial defect (for example, by modifying the size of a hole, or shifting a unit cell) that supports a resonant mode. A system which resembles the SSH model can be made by modifying this system to have alternating distances between the holes. Then, to create a topological defect for an edge mode, one side with unit cells whose holes are farther apart and one side where they're closer are brought together to make an interface. The Q-factor of this has been calculated numerically in the literature to be 59700 [42]. By designing varying bandgap sizes, the modal confinement was also found to be affected.

By taking two unit cells of an SSH chain, we can once again dimerize it to create more bandgaps (from the folding of the dispersion relation), which would include more edge states due to the opening of more bandgaps. This was realized by a linear array of optical waveguides, to form a kind of 'bowtie' lattice [43]. Mathematically, this means taking the square root of the initial Hamiltonian.

Chapter 5

SSH optical ring resonator implementation

In this project, we study the properties of the SSH model in an optical ring resonator, in particular the topological protection of an edge state. Physically, this is implemented by superimposing air holes over a standard ring resonator. The holes are then made to have alternating coupling separation distances. By itself, if a single type of unit cell (either trivial or topological) is present in the ring, no edge state will be supported. Thus, a ring can support two sites for edge modes, indicated by regions where there is a sudden change in the type of unit cell (either going from topological to trivial or vice-versa).

We will begin by examining the dispersion properties of the limiting case of the SSH waveguide, which will also allow us to carefully design the geometry of this system. By using those designs, we will then construct rings with them in order to quantitatively study the effect of various parameters. In particular, by using three proposed designs of varying bandgap sizes, we will introduce artificial defects to the bulk of the SSH chain in the ring and examine to which extent topological protection is still present. The results were obtained by numerically simulating the system in the frequency domain for the dispersion properties, and in the time-domain for the dynamical properties of the edge mode cavities.

5.1   Bandgap of the optical SSH waveguide

Before studying the SSH model implemented in an optical ring resonator with edge modes at constructed interfaces, we consider an infinitely long slab waveguide with a linear array of holes (with staggered separation distance). Doing so will allow us to see the bandgap opened by the increasing dimerization of the holes. In addition, by taking advantage of the scale-free nature of Maxwell's equations, a design approach can be employed to allow for complete control over the desired wavelength in the middle of the bandgap, all while giving us the geometrical features of the waveguide associated with such a wavelength.

The frequencies reported by both the Meep and MPB [44] software are 'unitless', in the sense that they remove the $2\pi c$ factor. So, for example, if a band structure or a resonant frequency reports a frequency of 0.645, then its wavelength is $1/0.645 = 1.55$. Then, the units of distance for that wavelength will match the units that is picked for the geometry (usually microns). This means that we can scale our geometry and the wavelength will scale similarly.

Let us assume that various geometrical features of a particular design (like the waveguide's width (w), radius of air holes (r), and the total length of the unit cell (L)). We can divide all of those features by the unit cell length, so that w/L, r/L, L/L and so on. This will also guarantee that the light cone will have a slope of unity. Then, we run the simulation and get a band structure. In order to properly scale the physical features to a desired wavelength λ

$$L' = \lambda \lambda' \tag{63}$$

With λ being the dimensionless wavelength reported by MPB's band structure (we can pick any point, for example the middle of a band gap), and λ' being the desired target wavelength (in our case, 1.55 microns) to be in the middle of the bandgap. We then must solve for L'. Then, we multiply again all of our geometrical features by L' (after being divided L, with rL'/L for the hole radius for example). With those new features, we can once again run the simulation, and we'll have the middle of the bandgap at the chosen wavelength (which will report e.g 0.645 instead) [45]. Those new features are what will be used to design a complete ring.

Figures 14, 15, and 16 show the calculated dispersion relations of the SSH waveguide for different sizes of bandgaps, whose structures will be the subject of the analysis of topological protection. The design methodology using the above scaling is explained in more detail in the following section.
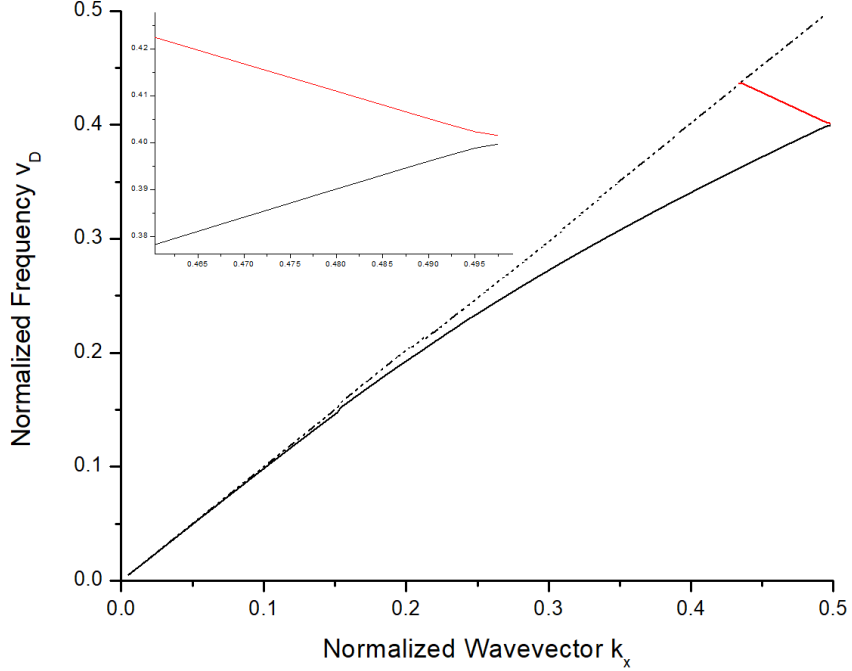
Figure 14: The dispersion relation of a weakly dimerized SSH waveguide. After normalizing to the target wavelength of 1.547μm for the edge state at the middle of the gap, it results in a bandgap that is 7nm wide.

5.2   Proposed designs of optical SSH waveguides

To design SSH optical waveguides (to be later made into rings), several constraints must be obeyed. In order to eventually fabricate these devices on a chip, the minimum feature size of fabrication process must be obeyed. For a typical optical lithography process, the smallest dimension must be less than 150 nm [46]. Of particular difficulty in this regard is the spacing between the air holes and edge of the waveguide $(w - 2r)$, the radius of air holes, and the distance between the air holes of the dimerization. This minimum feature size limits the extent to which the SSH waveguide can be dimerized, which results in small bandgap sizes (an important characteristic of topological insulators). By using an electron beam lithography process, this is

45
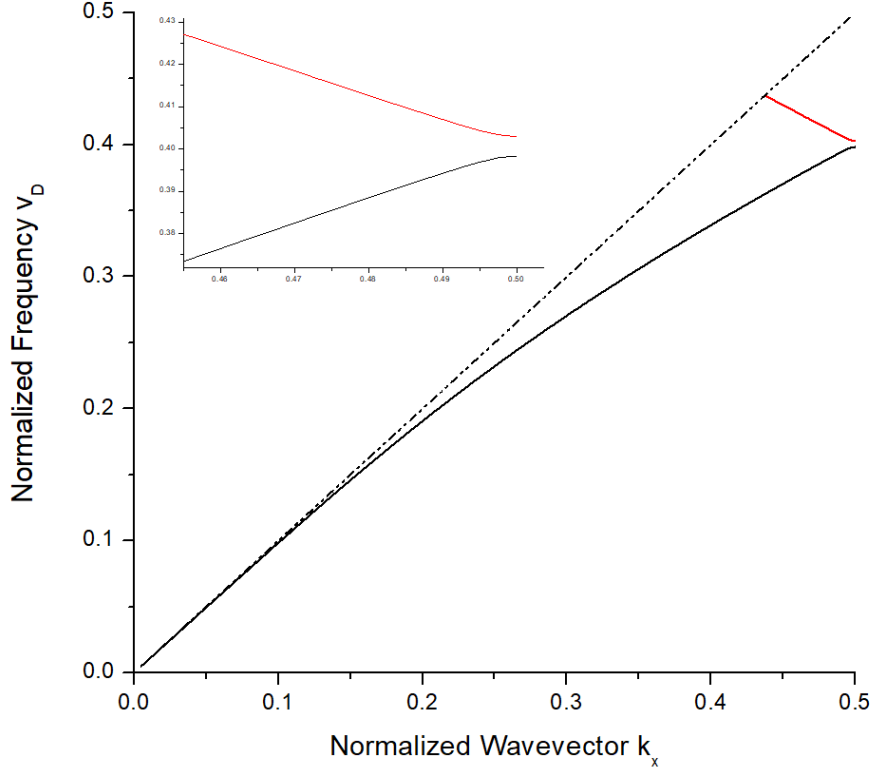
Figure 15: The dispersion relation of a moderately dimerized SSH waveguide. After normalizing to the target wavelength of 1.547μm for the edge state at the middle of the gap, it results in a bandgap that is 17.7nm wide.

somewhat mitigated due to allowing features down to 50 nm, which results in greater dimerization and bandgap sizes. These designs were nevertheless designed with the intent of fabrication with optical lithography, due to the high throughput and lower cost.

Another factor is that the position of the bands on the dispersion relative to the tip of the light-cone plays a role in the quality of the possible cavities that can be made. As the bands increase in normalized frequencies, more of the k-vector components couple to radiation rather than confined (guided or resonant) modes. This is due to the fact that less of each band is in the spectrum of guided modes. If there is more radiation, then the waveguides (and by consequence, the cavity which supports edge modes) will be more lossy.

Finally, the total length of the employed unit cell on the SSH waveguide also plays a role related to the aforementioned two, where a longer unit cell will again raise the
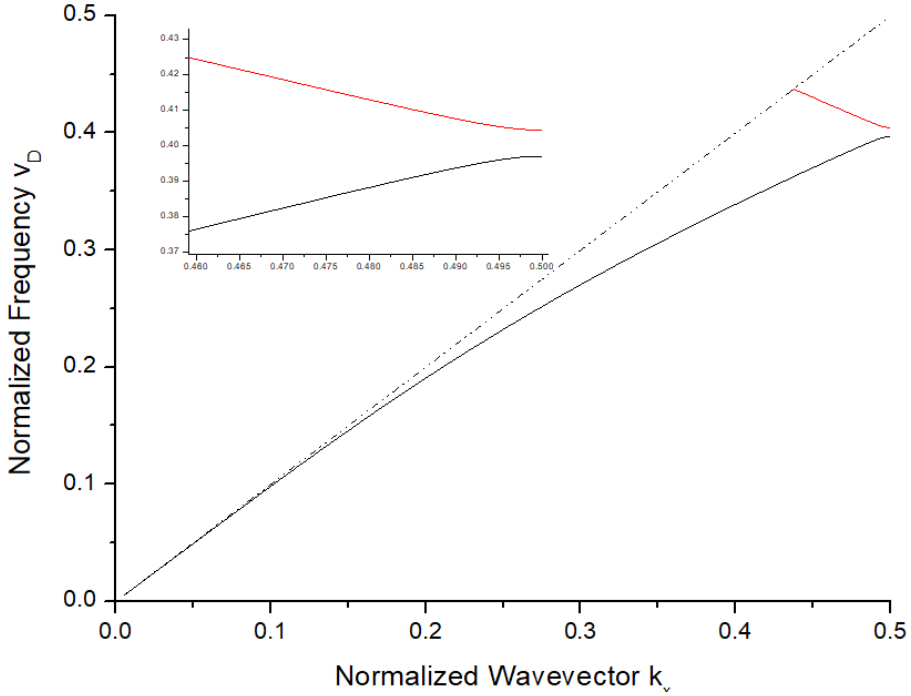
Figure 16: The dispersion relation of a strongly dimerized SSH waveguide. After normalizing to the target wavelength of 1.547μm for the edge state at the middle of the gap, it results in a bandgap that is 28nm wide.

bands closer to the tip of the light cone. The length of the unit cell depends on the two dimerization distances, a and b. This implies that the waveguide can only be dimerized to a certain degree if the minimum feature size is enforced

With all of these competing factors, three designs have been devised to attempt to obey the minimum feature size of optical lithography, while at the same time limiting coupling to radiation modes. These designs have their parameters summarised in table 4.

Previously, designs in silicon were attempted due to its higher index contrast. However, this is also a disadvantage, since it also results in raising the bands very close to the tip of the light cone (with dimensionless frequencies at around 0.45). Moreover, it also means that if were take an arbitrary design from a particular dispersion relation and scale its geometry according to the desired target wavelength of 1.547 μm, the resulting feature sizes are much too small to be fabricated, even with electron beam lithography. Small features are also undesirable since more leakage loss occurs. For
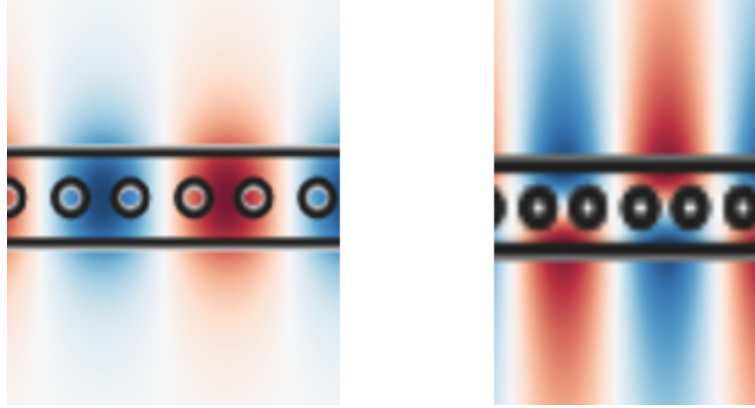
Figure 17: The B_z component of the field of the first and second bands, corresponding to the fundamental and higher ordered modes of the waveguide
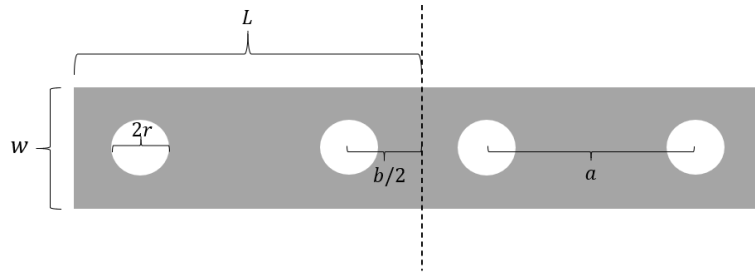
Figure 18: The SSH waveguide and its geometrical parameters. Its dimerization is governed by the difference of the a and b values.

these reasons, the silicon nitride platform was picked, due to allowing reasonable geometric features and adequate optical confinement. If opening the bandgap further is desired (and thus a longer unit cell length), a platform with an even lower index of refraction would be required.

5.3 Band inversion

An important feature of topology in periodic systems is the opening of a bandgap, where two bands can be separated by a topological invariant. Naturally, starting from an undimerized photonic crystal waveguide, a unit cell can be dimerized in two different ways, each with a different winding number. As per the band dispersion theory of optical waveguides, different bands will also have an associated field pattern (whether a fundamental mode with no nodes or higher ordered modes with nodes and a higher evanescent tail). As there are two different types of waveguides here (and two

	Weak dimerization	Moderate dimerization	Strong dimerization
a	0.32 μm	0.335 μm	0.35 μm
b	0.15 μm	0.1425 μm	0.135 μm
r		150 nm	
w		465 nm	
Bandgap size	7 nm	17.7 nm	28 nm
$n_{eff.}$		1.81	
Edge mode		1.547 μm	

Table 3: A summary of the parameters of interest for the three proposed designs of SSH waveguides.
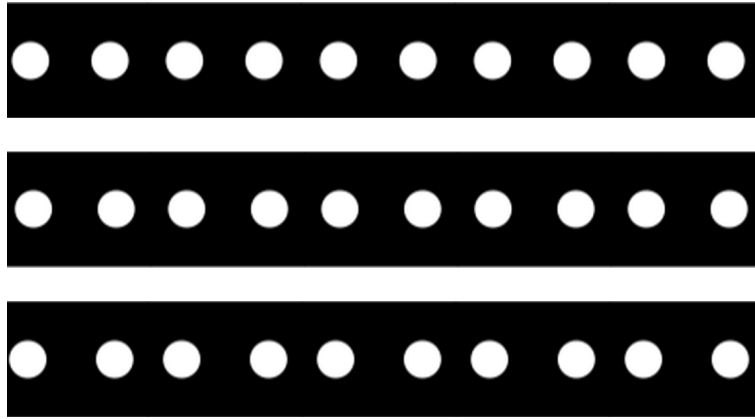
Figure 19: The dielectric functions of the weakly,moderately, and strongly dimerized SSH waveguides respectively..

types of dimerization), it implies that by performing a topological phase transition, a band will change its quantum state. This phenomenon of topological insulators is known as band inversion [47], which occurs when a system changes topological invariant and its quantum state is also changed. This occurs for the SSH model, even if the bulk lattice may appear the same upon inversion.

Figure 20 aims to show this property of topological band inversion, where for a particular waveguide configuration (either trivial or topological) each band is shown its field pattern. For example, initial, the first band can have the typical fundamental mode field profile and the seconde band has a field pattern with a node. Then, by switching the a and b geometrical parameters of the dimerization, as does the field patterns for both bands. This can be explained if we consider the waveguide and first turning undimerized (i.e, a photonic crystal waveguide) and then dimerizing again.
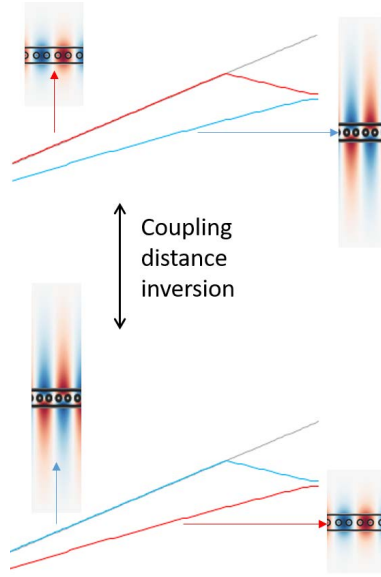
Figure 20: By inverting the two coupling distances, a and b, of the dimerization of an SSH waveguide, the mode profiles of the two bands will also switch accordingly.

5.4 Analysis of topological protection at the edge state

5.4.1 Effect of disorder and gap strength

In this model, due to the ring's imposed periodic boundary condition (in other words, as a travelling wave does a full circuit around the ring, it will keep experiencing the ring's effective index), it can serve to emulate an infinite chain required from the theoretical model. In order to close the ring properly, two topological defects need to exist. If the two topological defects are brought closer together, splitting of the edge modes can occur (due to coupled-mode theory) and interesting phenomena may be possible.

The core of this work is to geometrically design robust optical cavities in the SSH model in a ring formation and examine the extent of topological protection on these edge states. The latter will be accomplished by taking the three previously outlined designs and subjecting them to certain degrees of defects on the lattice. Specifically, the radii of the air holes will be made to vary according to a random gaussian distribution, with an increasing variance.
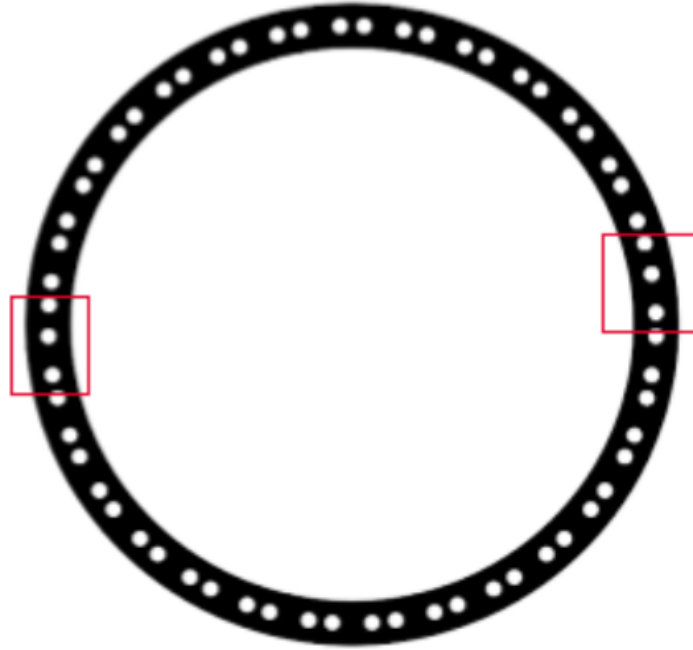
Figure 21: The dielectrinc function of the SSH model implemented in a ring resonator. The topological phase transitions (which supports the edge modes) are denoted by the red boxes, and are at the interface between a chain of trivial and topological unit cells, or vice-versa.

Prior to obtaining numerical data, significant convergence testing on the system was performed [48]. When simulating a physical system using numerical methods, certain parameters serve only increase the final accuracy, up to a point. In order to verify the accuracy of any numerical model, convergence testing is performed by continually increasing the value of the convergence parameters until a desired tolerance is acquired (in practice, this is accomplished by comparing two results and verifying that they do not change significantly). In this project, the convergence parameters and the width of the PML, the air padding between the ring resonator and the PML surface, the spatial and temporal resolution, and the runtime used to measure the fields and extract the resonant mode information. The air padding contributes to the solutions accuracy due to the fact that, if small enough, the outgoing waves may not hit the PML surface at a normal angle, which will incur additional undesirable reflections. If the width of the PML is small enough, the incoming light may not decrease in amplitude enough, which could result in some of the light going back to the computational domain. Typically, a PML width of up to twice the largest wavelength is used. In order to
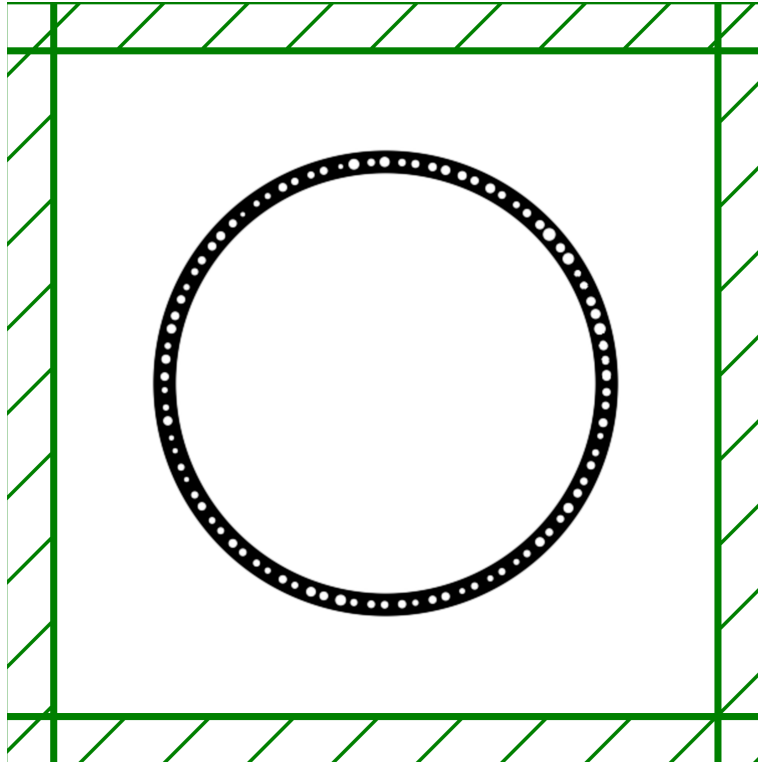
Figure 22: An example of a typical computational domain used to study the topological cavities. Here, disorder was purposfully introduced to the holes of the unit cell. The green border represents the PML.

obtain enough time-domain data on the fields and obtain a good Fourier response for resonant modes, and high temporal resolution is also required. Any simulation serves only as an approximation to a real physical problem, which means that in order for a computer to approximate a solution, the domain must be discretized according to a grid. As the spatial resolution is increased, the field data is solved at more 'pixels', resulting in a more accurate solution, at the cost of a much increased simulation time. However, a high enough resolution is also required to approximate curved surfaces, such as circles. In the Meep software, a subpixel smoothing scheme is used [49], which uses perturbation theory to approximate the interface of two materials and reduce staircasing artifacts. Overall, for the simulations in this project, the following convergence parameters were found to provide both reasonable simulation time and high accuracy: resolution of 40 pixels per μm, PML width of 3 μm, air padding of 5 m, and a runtime of 100 Meep time units.

The following plots in figures 23 and 24 show when each designed cavity has the

property of topological protection under the influence of disorder induced by the air holes. Both the Q-factors and resonant wavelengths remain constant until that point, until they start decreasing and randomly fluctuating respectively. For each points in these plots, a total of 10 simulations were performed to obtain a representative sample.

Recall from the theory of topological insulators that a requirement for protected edge states is that the gap remains open even when influenced with perturbations. This implies that by opening the bandgap more greatly, the edge states could sustain higher degrees of disorder, due to it becoming more difficult to close. Indeed, this is reflected here, where the SSH design with the greatest degree of dimerization (opening the bandgap to the greatest value found of 28 nm) has been found to retain its mode quality to a high percentage. The opposite also follows for the design with the smallest bandgap of 7 nm.

A peculiar finding is that the SSH design with the moderate dimerization was found to possess the highest Q-factor of the studied cavities. A possible explanation for this is by considering the losses in the lattice and radiation in air in relation to the size of the bandgap. For a larger bandgap, while localization of the light in the cavity may be greater, it leaves more room for light to leak outside of the ring in the form of radiation, having an adverse effect on the mode's quality. On the other hand, for a smaller bandgap, localization in the cavity may be lessened, which could mean that more light is able to leak in the remaining lattice, and less so as radiation. This implies that there may be a trade-off between the two in order to balance the Q-factor. As such, the cavity with the moderate dimerization aims to reduce both to a minimum and serve as a compromise.

To verify the claim that edge states can endure perturbations in the lattice, the same results were also obtained for the same system, but for a trivial defect (commonly seen in nanobeam cavities). Here, to create localization of light, instead of abruptly having a change in topological invariant, the same type of lattice (either topological or trivial) is used throughout the entire ring. Then, the radius of the air holes of a single unit cell is reduced from 150 nm to 50 nm. Just as before, a gaussion pulse is launched slightly off-center in this defect. For all three designs, the Q-factors, while their starting values are comparable to the unperturbed topological defects,
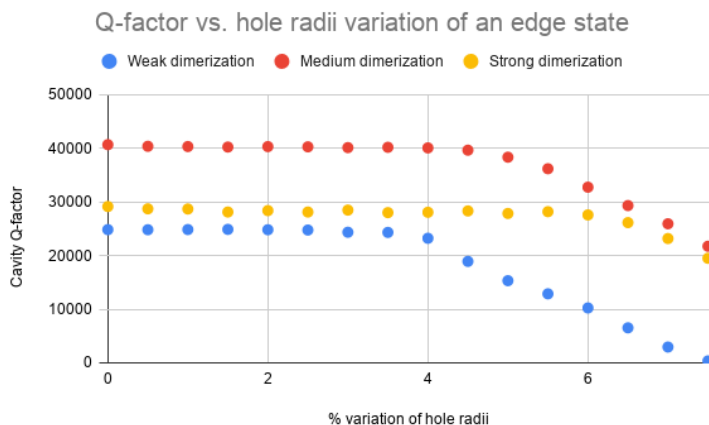
Figure 23: The evolution of the cavities' Q-factors as the bulk lattice is perturbed (by randomly varying the hole radii) of the edge state. For the weak dimerization, topological protection occurs until a hole radii variation of 3.8%, for the moderate dimerization it occurs until 5.6%, and it occurs at 7.7% for the strong dimerization.

nevertheless begin to degrade nearly immediately. The resonant wavelengths also experience large variance much earlier.

	Weak dimerization	Medium dimerization	Strong dimerization
Q-factor	24840	40502	28820
Protection	3.8%	5.6%	7.7%
Bandgap size	7 nm	17.7 nm	28 nm

Table 4: A summary of the main results of the properties of the topological cavities for the three proposed designs of SSH ring resonators.

5.4.2   Effect of resonator curvature

In a standard ring resonator configuration, as its radius increases, so does the optical confinement. This can be attributed to the mechanism of total internal reflection: the critical angle condition is more easily met for a waveguide with less bending. For the studied structure of the SSH waveguide in a ring formation, instead of whispering-gallery modes, the resonance is localized in a defect by a photonic crystal waveguide superimposed on the ring.

As the radius of the three types of resonators are increased, so do the Q-factor. This is mainly attributed to the fact that leaking of light is facilitated on a lower bending radius. Recall the previous required approximation that the radius be much larger
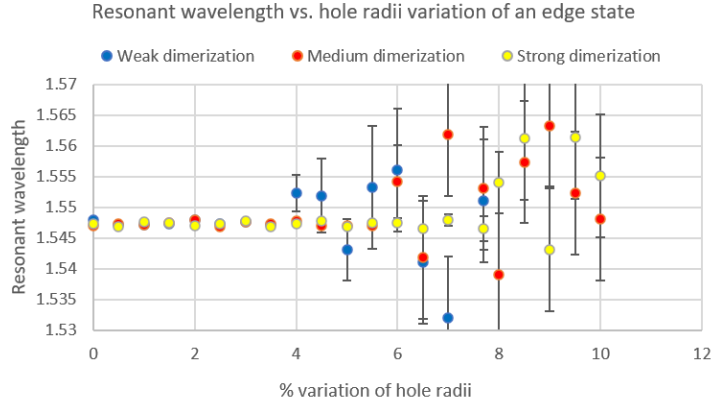
Figure 24: The fluctuation in wavelength of the cavities' as the bulk lattice is perturbed. After topological protection no longer occurs, the resonant wavelengths are no longer robust, and can greatly vary from different simulations.

than the operating wavelength of the resonant mode. For smaller radii, the diffraction loss dominates (not unlike the whispering-gallery modes of a standard ring resonator), and the approximation of a straight waveguide breaks down.

On the other hand, as the radius increases, the ring system asymptotically approaches the case of an optical nanobeam cavity in a straight waveguide. Here, every component of the k-vector is fully coupled to the entire waveguide (compared to having curvature, where some of the k-vector will couple to radiation modes). Much work has been done on the nanobeam cavity in a photonic crystal waveguide in order to optimize its Q-factor.

5.4.3 Quantitative analysis of loss mechanisms

Inherent in any optical system is loss. In this studied system, two main loss mechanisms exist, in the form of radiation leakage into the air (not unlike whispering-gallery-modes in standard ring resonators), and leakage out of the created defected into the rest of the lattice (which is typical of nanobeam cavities).

While topological protection of edge states cannot truly remove sources of optical loss, it can mitigate the addition of further loss created by small defects. Since the periodicity and topological phase transition is imposed on the lattice, the optical cavity should only be robust to imperfections created on the lattice. This also means
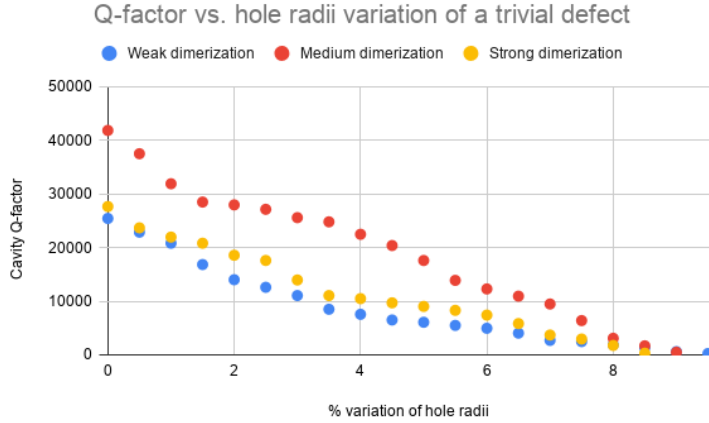
Figure 25: The evolution of the Q-factors of the trivial cavities as the hole radius variation increases. Without topological protection, the Q-factors rapidly decrease.

that radiation leakage should only be noticed after enough imperfections are added to close the bandgap, and bypass topological protection. However, for radiation leakage, since air is only topologically trivial, there does not exist edge states in this direction. As such, the two loss mechanisms can be said to act independently on the cavity, where topological protection does not effect the radiation leakage.

As a test that topological protection is indeed present, the incoming electromagnetic flux was measured both in the lattice, far from the topological defect to measure the leakage lost in the remaining lattice, and in the air to measure the radiation leakage. For the former, it was found that the point at which significant flux is measured (and when this loss mechanism starts to dominate) matches the previous findings on the cavities' Q-factors.
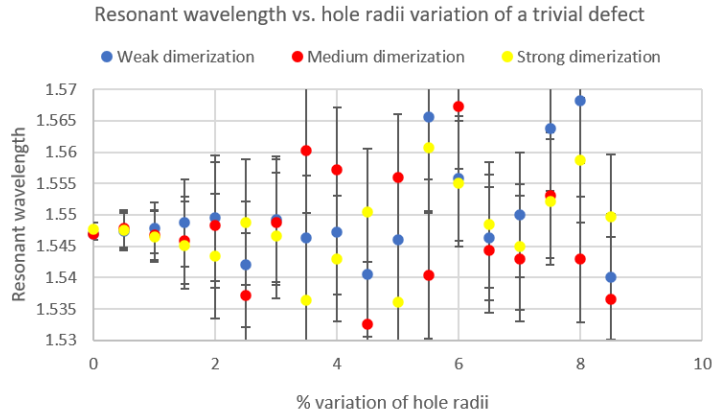
Figure 26: The fluctuation in wavelength of the trivial cavities as the bulk lattice is perturbed. Nearly immediately, the wavelength variance of the multiple conducted simulations is high.
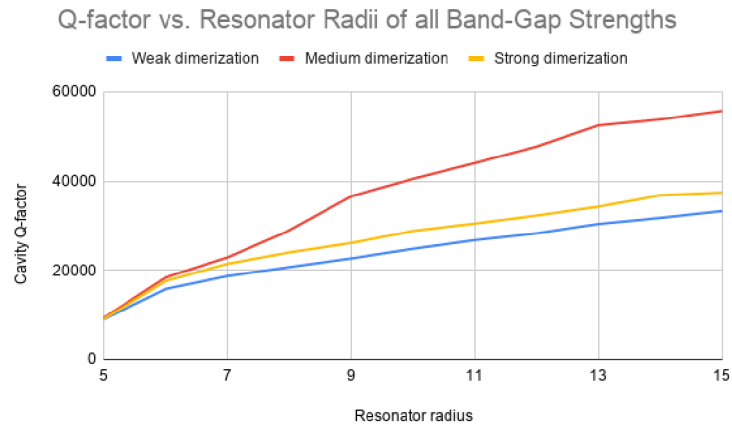
Figure 27: The Q-factor of the topological cavities as a function of the radius of the ring resonator. As the radius increases, the ring approaches the limit of the cavity in a straight nanobeam.
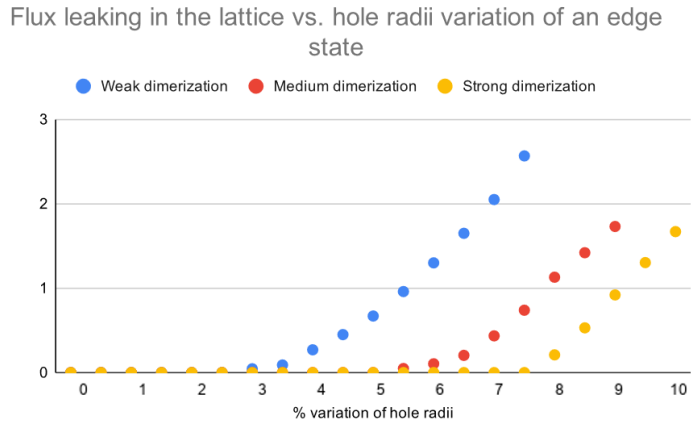
Figure 28: The measured unitless flux in the ring as the hole radius random variation is increased. After topological protection (which matches the previous findings), the light starts leaking into the rest of the ring's lattice.
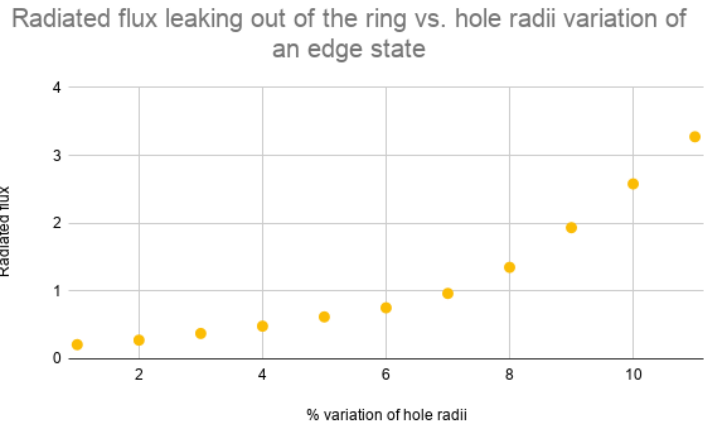
Figure 29: The measured unitless flux in air (from, the cavity the strong dimerization), far from the ring as the hole radius random variation is increased. Since air is only topologically trivial, this loss mechanism is unrelated to the loss in the ring, and is not immune to the topological protection created by the interface in the lattice.

Chapter 6

Proposed experimental testing

6.1 Silicon-on-insulator platform

Devices etched on a silicon wafer is the main way to create electronic circuits. By using a well understood and inexpensive material, silicon, it is possible to construct devices which are the backbone of the electronics industry. Decades of development has already been invested in developing these processes. As such, the photonics industry has a mature platform readily available to leverage.

As a matter of fact, silicon has desirable optical properties, making it a good candidate material for the operation of photonic integrated circuits. It has a high index of refraction ($n = 3.5$ at the telecommunications wavelength, 1.55 μm), allowing high optical confinement in waveguides or resonators when surrounded by a lower index cladding, such a silicon dioxide ($n = 1.44$). Silicon is also transparent in the infrared spectrum, allowing signals to propagate long distances in optical fibres with no attenuation.

To fabricate silicon devices on a chip, the silicon-on-insulator platform is commonly used [50]. A 220 nm thick layer of silicon (where the geometry of the devices are etched) is deposited on top of a 2 μ m thick layer of silicon dioxide (commonly referred to as 'buried oxide'). A cladding of silicon dioxide on top of the silicon layer is also possible. These photonic devices are fabricated using CMOS compatible processes, allowing the designer high flexibility and feature sizes down to 50 nm.
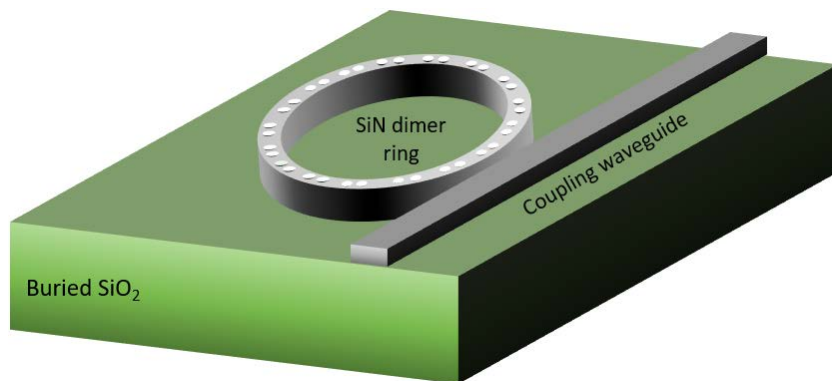
Figure 30: The SSH ring resonator implemented on the nitride platform. The ring and coupling waveguides are made of silicon nitride, on a substrate of silicon dioxide.

Recently, alternative platforms for optical devices have been explored. One such material is silicon nitride [51]. It is another CMOS compatible material with a somewhat lower index of refraction ($n = 2$). While the optical confinement is lesser compared to silicon, having a higher index than silicon dioxide allows it to nevertheless confine light in waveguides. Its lower index of refraction makes it less sensitive to scattering losses in the presence of fabrication defects. Waveguides and ring resonators can also be made to have larger dimensionality without exciting higher order modes, which could allow devices with even lower losses to be conceived. The nitride layer is made to have a height of 440 nm on top of the buried oxide layer. Like silicon, it is transparent in the infrared spectrum, and visible in the mid-infrared range.

The silicon on insulator platform, however, has some inherent sources of optical loss. For one, two photon absorption, which occurs when two photons are absorbed by the material, introducing losses beyond our control. From a fabrication perspective, the etching process of the silicon layer introduces some small imperfections on the sidewalls of the devices. As a result, this creates scattering losses out of the device. However, as fabrication foundries improve upon their process, smoother sidewalls can eventually be made.

6.2   Microfabrication techniques

The creation of photonic devices on a chip depend on the ability to etch out geometries on a silicon layer with great precision. Currently, there are two main techniques

employed for this process: electron-beam or optical lithography. Both processes use a similar series of steps for the fabrication. To start, a layer of resists is applied on top of the silicon layer which is then exposed to the pattern of our desired devices. The device is then etched in the silicon layer down to the substrate. The remaining resist layer gets removed, and a lower index cladding is possibly superimposed on the device layer. Multiple etching layers are also supported, making the fabrication of devices such as grating couplers and rib waveguides possible. For advanced devices with active components, metal contacts for heating is supported, as is ion doping. These allows for more advanced devices, such as ring modulators, and being able to tune the resonances by silicon's thermo optic coefficient.

Electron-beam lithography allows for much smaller minimum features size (around $50nm$) to be accomplished, making it a high precision technique [52]. This is important for devices whose operation depend on small features, such as Bragg gratings. This is accomplished due to the beam's direct patterning of the devices on the resist. However, due to the beam's requirement to scan every 'pixel' of the wafer, the fabrication process is slow. It is also expensive. Both of these factors often make electron beam lithography undesirable for rapid prototyping and manufacturing.

On the other hand, optical lithography uses a mask that's already been patterned with the device layout [53]. While increasing the allowable resolution and minimum features sizes (allowing for 150 nm), its high throughput is more desirable to fabricate many devices quickly. However, more care must be taken in designing the devices such that the minimum feature size is not violated.

6.3 On-chip testing

The SSH ring resonators were designed as to be testable on the nitride platform. A cavity of the SSH ring resonator can be placed in proximity to a waveguide of width 1 μm, such that by evanescent coupling, the mode will enter the cavity. Then, the light in the waveguide can in principle be measured for its transmission spectrum, with features such as the bandgap and edge mode resonance appearing. While this light can be generated by a laser going into an optical fiber, the modal mismatch due to the physical difference the fibre and optical waveguide makes this coupling challenging. To inject light into a photonic integrated circuit, a device known as a

grating coupler is used. It uses a bragg grating to couple vertical modes [54]. To minimize reflections out of the device, the optical fiber is aligned at an angle from the grating coupler Once the light is coupled to the grating coupler, it then goes to a waveguide and into the rest of the circuit. This mode conversion can be made to occur with minimal insertion loss.

This can be used for our devices by placing both an input and output grating coupler on the ends of a waveguide coupled to the ring resonator. The grating couplers should be placed far enough from each other such that undesirable interactions and reflections are prevented.
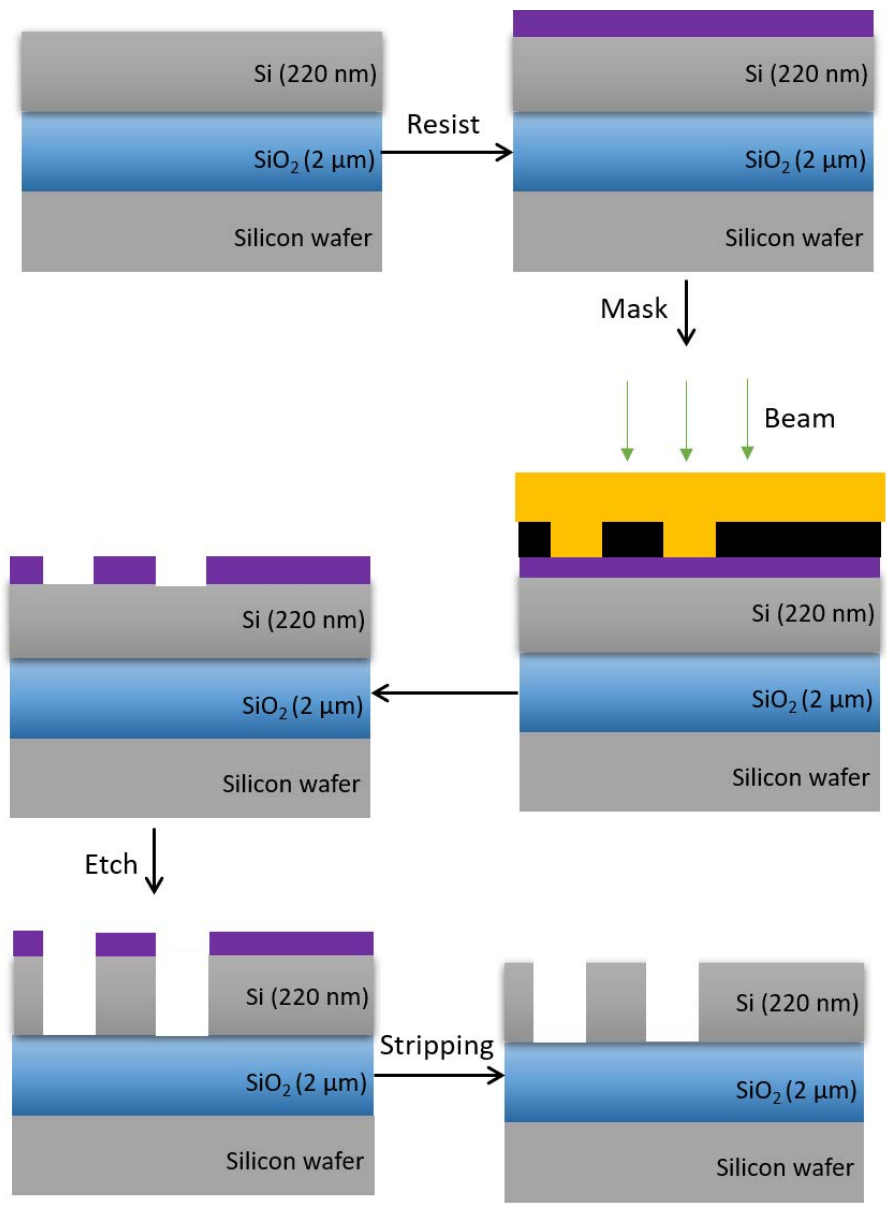
Figure 31: The steps involved in a lithography process for a silicon chip.
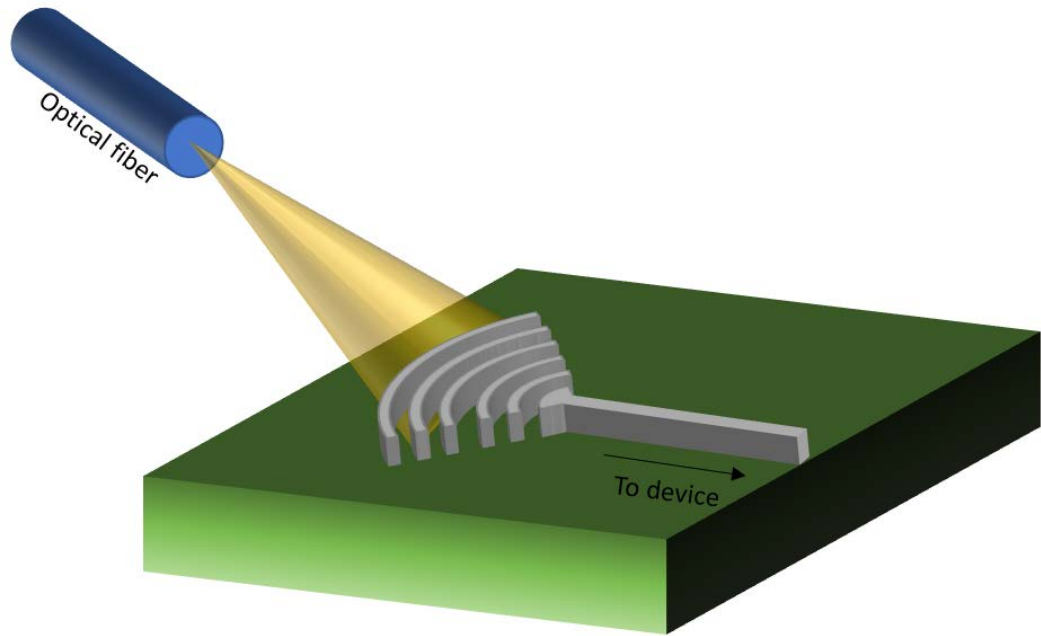
Figure 32: Light from an optical fiber being coupled to a photonic integrated circuit by using a grating coupler.

Chapter 7

Conclusion and outlook

Evidently, the field of topological photonics introduces exciting research directions
in the context of fabricated integrated devices. In particular, the analogies between
optics and quantum mechanics imply that there are many possibilities for systems and
concepts to explore in photonics, and to discover how far we can take the comparisons.
To this end, there are a several possibilities for future research projects related to this
topic. A few of interest are outlined below:

1. **Photonic topological insulators on-a-chip.** As shown, the great techno-
   logical progress of silicon foundries can be directly applied to fabrication of
   photonic circuits. This can open a whole new field of research where systems
   from topological condensed matter can be engineered by periodically engineer-
   ing a photonic structure [55]. In particular, more one dimensional models could
   be implemented in a ring resonator, similarly to the work of this thesis. For
   example, additional edge states could be engineering by dimerizing the waveg-
   uide lattice again, which would 'fold' the dispersion relation and open a new
   bandgap. A two dimensional square lattice could also be dimerized to procude
   edge states at the boundary.

2. **Exploring bound states in the continuum and symmetries.** In eigen-
   value problems, solutions can either belong in the discrete spectrum of real
   solutions where the allowed fields are localized, or they can belong to the con-
   tinuous spectrum of plane waves, where an infinite number of solutions are not
   restricted by discreteness. However, it has been reported that those discrete

solutions may indeed exist in this continuous spectrum [56], even if the problem's geometry does not permit it. One way to achieve this is by decoupling different symmetry classes. While this effect was originally studied in quantum mechanics for the von Neumann and Wigner potentials, it could also be realized in optics. In waveguides, beyond the light cone lies the continuous spectrum of radiation modes. By using this phenomenon, we could realized guided modes that exist in the dispersion relation beyond the light cone. It is suspected that the SSH model possesses the necessary symmetries for this property. More frequency domain simulations of bands above the light cone are required to test this hypothesis.

3. **Synthetic dimensions in photonics.** A system's apparent physical dimension is dictated by its geometry. For example, a single resonator represents a zero dimensional system, a linear array (consisting of multiple coupled resonators) represents a one dimensional system, and a planar lattice represents a two dimensional system. However, beyond this point, photonic integrated circuits cannot support higher physical dimensions, which prevents us from exploring the properties of three dimensional or higher systems. By engineering the various degrees of freedom of our system, we could realize a higher dimensional system compared to its physical dimension [57].

To conclude, this work presented a quantitative analysis of the SSH model in an optical resonator. We first outlined the design process of the cavities in these rings, and verified that these waveguides do indeed exhibit topology by verifying that the bands' modes were inverted when the dimerization coupling distances are flipped. With numerical simulations, the full extent of topological protection was put to the test. By artificially adding random variations to the holes of the lattice, the Q-factors of the cavities were shows to remain constant with a relatively high level of imperfection. It was found that we can increase the effect of topological protection by widdening the system's bandgap, making it harder to deform and close/reopen. To confirm that further loss into the lattice is mitigated, the radiated power in the ring and air were measured, and stayed consistent with previous our findings.

This shows promise for the future of photonic integrated circuits, since we could in principle have a counter against the ever-present and undesirable effects of lithography

induced defects by creating a topological edge state. Applications which depends on guiding of light and high Q-factor/precise resonance location in particular would benefit from this new field. However, creating a topological edge state is expensive in device real estate, since we must create two bulk lattice to realize an interface.

Finally, we briefly discussed a potential approach to experimentally test these devices if they were to be fabricated using the silicon nitride platform. By measuring the transmission spectrum by means of light from an optical fiber being sent to a grating coupler, and ultimately onto a bus waveguide coupled to these rings, we could directly witness the bandgap created, as well as the edge mode at the middle of this bandgap.

Appendix A

Mode coupling in optical ring resonators

We previously considered only general properties of the ring resonators and its conditions on resonance. In order to calculate its transfer characteristics as a filter, we must calculate the ratio of the power transferred at the exit port a waveguide. The ring resonator coupled to a bus waveguide can be considered as a four port network [58]. To simplify the analysis, we shall assume the coupling to be lossless, and only a single polarization is possible. The interactions of the field amplitudes at the various ports can be written as:

$$
\begin{pmatrix} E_{t1} \\ E_{t2} \end{pmatrix} = \begin{pmatrix} t & \kappa \\ -\kappa^* & t^* \end{pmatrix} \begin{pmatrix} E_{i1} \\ E_{i2} \end{pmatrix}
\tag{64}
$$

With t being the 'self' coupling coefficient of the waveguide of ring, and κ being the coupling coefficient from the ring. This device is reciprocal from the symmtry of the matrix. For lossless coupling, this relation holds true:

$$
\left| \kappa^2 \right| + \left| t^2 \right| = 1
\tag{65}
$$

The incoming wave amplitude, E_{i1}, can be unity. After experiencing a roundtrip around the ring, which may have loss mechanisms described by the coefficient α, the field amplitude also experienced a phase shift described by:
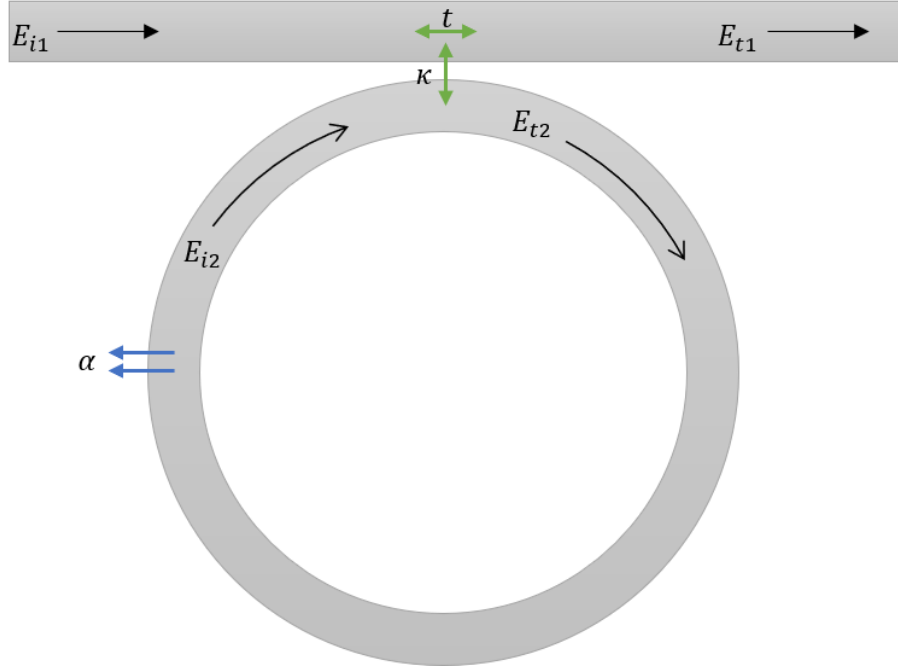
Figure 33: The theoretical model of an optical ring resonator, using a transfer matrix approach to treat the device as a four port network. The ring has inherent loss according to α, coupling coefficientd κ and t, and field amplitudes in the four regions.

$$E_{i2} = \alpha \cdot e^{j\theta} E_{t2} \tag{66}$$

We can introduce the effective index of the ring experienced by the wave by the following relation:

$$\beta = k \cdot n_{\text{eff}} = \frac{2\pi \cdot n_{\text{eff}}}{\lambda} \tag{67}$$

With the propagation constant of the wave, we can rewrite its phase function in terms of this effective index and operating wavelength, which is expressed as:

$$\theta = \frac{\omega L}{c} = \frac{k c_0 L}{c} = k \cdot n_{\text{eff}} \cdot 2\pi r = \frac{2\pi \cdot n_{\text{eff}} \cdot 2\pi r}{\lambda} = 4\pi^2 n_{\text{eff}} \frac{r}{\lambda} \tag{68}$$

By inserting the expression of the wave experiencing a loop of the ring into our initial network matrix, the remaining wave amplitudes can be solved. For the wave being transferred to the output port of the waveguide, its amplitude is:

69

$$E_{t1} = \frac{-\alpha + t \cdot \mathrm{e}^{-\mathrm{j}\theta}}{-\alpha t^* + \mathrm{e}^{-\mathrm{j}\theta}} \tag{69}$$

For the wave being coupled from the input port of the waveguide to the ring, its amplitude is:

$$E_{t2} = \frac{-\kappa^*}{1 - \alpha t^* \mathrm{e}^{\mathrm{j}\theta}} \tag{70}$$

By using the above amplitude and replacing it in our initial guess of the wave after experiencing a full loop, we can rewrite it:

$$E_{i2} = \frac{-\alpha \kappa^*}{\alpha t^* + \mathrm{e}^{-\mathrm{j}\theta}} \tag{71}$$

Equipped with all amplitudes in the network, we can then easily calculate how much power is being transferred to the exit port of the waveguide as a function of the operating wavelength, giving us the ring's spectral characteristics. To obtain the power of a particular field amplitude, we can take its magnitude squared. As such, the power circulating in the ring, representing the ring's supported resonances, is:

$$P_{i2} = |E_{i2}|^2 = \frac{\alpha^2 \left(1 - |t|^2\right)}{1 + \alpha^2|t|^2 - 2\alpha|t|\cos\left(\theta + \varphi_t\right)} \tag{72}$$

Similarly, we can calculate the power transferred to the exit port of the waveguide, after the wave experiences a waveguide to ring coupling, a full circuit around the ring, and ring to waveguide coupling. This represents the ring's spectrum:

$$P_{t1} = |E_{t1}|^2 = \frac{\alpha^2 + |t|^2 - 2\alpha|t|\cos\left(\theta + \varphi_t\right)}{1 + \alpha^2|t|^2 - 2\alpha|t|\cos\left(\theta + \varphi_t\right)} \tag{73}$$

We can clearly see the equidistant dips along the spectrum, corresponding to all of the free spectral ranges of the ring to be equal. The dips represents the ring's resonant wavelength, where the condition that an integer number of wavelengths can fit around the ring is met. While this physical interpretation was easily reasoned in chapter 2, we more rigorously calculated the transfer function here. This powerful method can also be generalized to include a second bus waveguide to have a ring in

an add-drop configuration. If the loss parameter of the ring α can be made close to unity, very high Q-factor can be achieved. Graphically, this is represented by the dips being made sharper. Again, an equivalent approach was argued by means of the Fourier transform of the wave decaying in the time-domain, where the linewidth of the resulting Lorentzian determines the Q-factor of the resonator.

Figure 34: A standard transmission spectrum of an optical ring resonator coupled to a bus waveguide. The plot shows resonances that are equally distanced.

In a pratical device, it may be desirable for as much of the power possible to be transferred from the waveguide to the ring. By coupled-mode theory, this power transfer can be controlled by the coupling coefficients of both the ring and waveguide κ and t. In practice, this is accomplished by modifying the physical gap between the ring and waveguide. For a large enough gap, no coupling of power occurs, since the evanescent field of the waveguide could not extend to the ring. On the other hand, if the coupling gap is made to be too small, even though a coupling of power would occur, this would incur insertion loss.

In order for the all of the incoming power to be transferred to the ring (and consequently, for the resonance dips to reach 0), a certain condition on the coupling coefficient t and loss coefficient α must be met. There as three such regimes for the ring.

For a ring with resonances reaching a transmission of zero, which is also in the regime known as critical coupling, the necessary condition on the two parameters is:

$$\alpha = |t| \tag{74}$$

Otherwise, if α is made greater or less than t, the ring is said to be overcoupled (where insertion loss is significant)and undercoupled (where the coupling gap is small enough to not have optimal power transfer from the waveguide to the ring), respectively. In both cases, the dips of the resonances do not reach zero, indicating an incomplete transfer of light in the waveguide.

Appendix B

PWE and FDTD numerical methods

The results obtained in this work were done by means of numerical simulations. Namely, the finite difference time domain method was used to calculate the spectral response of optical resonators, where a Gaussian source is injected in the cavity and the resonances are measured by a signal processing approach. As well, in order to model the dispersion relation of the SSH waveguides, a frequency domain approach for solving the eigenvalue problem was used. This frequency domain approach imposed periodic boundary conditions in every direction along the points of high symmetry, making it possible to model such periodic structures. Both of the approaches will be outlined in this appendix.

The finite difference time domain is a powerful numerical technique which lets us calculate a wide range of devices and phenomena, for a variety of material types. By having direct access to the calculated field data, many different types of calculations can be accomplished, such as radiated power, loss, etc. This method is also easy to understand and implement, requiring no linear algebra. However, it can be a potentially slow method, due to the timestepping nature of the algorithm. In addition, a high spatial resolution of the discretization is required to obtain accurate results.

In order to discretize Maxwell's equations and the computational domain, we use the
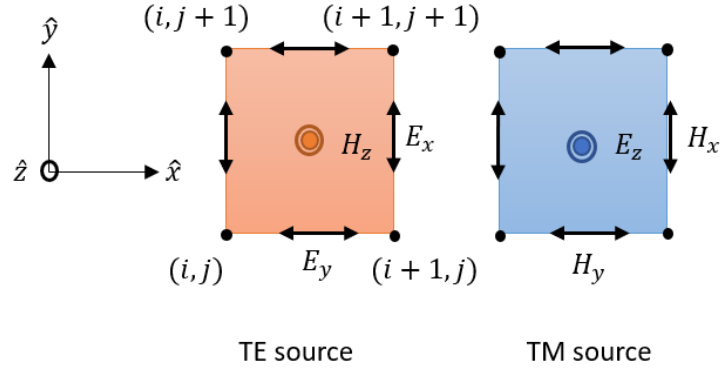
Figure 35: A single Yee grid unit for the discretization scheme for a two dimensional computational domain. Different z-component fields are calculated depending on the input source.

Yee grid [59], where we simply have a square grid of points at locations where the field data is calculated. The Yee grid's usefulness arises in allowing us to calculate the **E** and **B** components at different points. For a particular point in space, this discretization can be expressed as:

$$(i, j, k) = (i\Delta x, j\Delta y, k\Delta z) \tag{75}$$

with Δx, Δy, and Δz being the grid's incremental distance. For accurate solutions of numerical simulations, having a high spatial resolution (corresponding to having many grid points) is critical. However, a consequence of discretizing the problem as an array is that 'staircasing' effect, which occurs when curved surface cannot be described accurately by a grid. In practice, schemes based on perturbation theory which serve to smooth the surfaces of the permitivity tensor have been employed.

In order to fully describe the fields' dynamics, we also discretize the time by a similar scheme. By inserting the discretized spatial and time evolution of the grid, a function can this be rewritten as:

$$u(i\Delta x, j\Delta y, k\Delta z, n\Delta t) = u_{i,j,t}^n \tag{76}$$

Yee's expression for a discretized spatial derivative for a coordinate can be derived to be:

74

$$\frac{\partial u}{\partial x}(i\Delta x, j\Delta y, k\Delta z, n\Delta t) = \frac{u_{i+1/2,j,k}^n - u_{i-1/2,j,k}^n}{\Delta x} + O\left[(\Delta x)^2\right] \qquad (77)$$

A similar idea can be applied to the time derivative:

$$\frac{\partial u}{\partial t}(i\Delta x, j\Delta y, k\Delta z, n\Delta t) = \frac{u_{i,j,k}^{n+1/2} - u_{i,j,k}^{n-1/2}}{\Delta t} + O\left[(\Delta t)^2\right] \qquad (78)$$

These discretized functions can be inserted in any variation of Maxwell's equation. Then, by initializing the simulation with a source to serve as an initial condition, the field components can be calculated at any physical point in the Yee grid, for all future times.

As with any physical system, a computational domain must be backed by a boundary condition. The domain can be backed by a perfect electrical conductor, which would result in the waves being reflected. Periodic boundary can also be implemented, where by introducing a proper wavevector, a wave entering one side would exit another. Most commonly employed in wave propagation problems is the backing of a perfectly matched layer (PML), which serves to simulated an 'open' domain, as if the waves were radiating to infinity [60]. This is physically implemented by having region with some thickness and having a permitivity function described by an lossy, tensor valued permitivity function which absorbs incoming waves for a wide range of incident angles. However, care must taken such that the boundary of the PML is far enough from the structures so it does not interfere with any evanescent fields, since additional reflections will occur.

Let us now consider the more specific case, of a periodic dielectric function whose fields obey Bloch's theorem as seen in chapter 3. A frequency-domain eigenvalue solver for Maxwell's wave equation can be used to calculate for the unit cell's allowed field patterns and bands/frequencies (which, in general depend upon the wavevector) [61]. With Bloch's theorem inserted in the electromagnetic master equation, the

$$\left[(i\mathbf{k} + \nabla) \times \frac{1}{\varepsilon(\mathbf{r})}(i\mathbf{k} + \nabla)\times\right]\mathbf{u_k}(\mathbf{r}) = \hat{\Theta}_\mathbf{k}\mathbf{u_k}(\mathbf{r}) = \frac{\omega(\mathbf{k})^2}{c^2}\mathbf{u_k}(\mathbf{r}) \qquad (79)$$

Thus, the calculation need only be performed on a single unit cell, together with the proper lattice vectors. Together with the constraint from Gauss's laws', our problem

can uniquely be defined:

$$(i\mathbf{k} + \nabla) \cdot \mathbf{u_k} = 0 \tag{80}$$

We now wish to extract the eigenmodes and dispersion relation. By taking advantage of the periodicity, a spectral method based on a plane wave expansion can be employed. To illustrate this calculation, note that any periodic function can be expanded as an infinite sum of plane waves, by a Fourier series:

$$u_k(x) = \sum_{n=-\infty}^{\infty} c_n(k) e^{i\frac{2\pi u}{a}x} \tag{81}$$

Generalizing this further, we can instead use the reciprocal lattice vectors of the physical space lattice vectors of a lattice. Its associated Fourier series is:

$$\mathbf{u_k(r)} = \sum_{\mathbf{G}} \mathbf{c_G(k)} e^{i\mathbf{G} \cdot \mathbf{r}} \tag{82}$$

Given this Fourier series representation of the field's envelope function, by direct substitution in the electromagnetic eigenvalue problem equation

$$\sum_{\mathrm{G}} \left[-\varepsilon_{\mathrm{G'-G}}^{-1} \cdot (\mathbf{k} + \mathbf{G'}) \times (\mathbf{k} + \mathbf{G}) \times \right] \mathbf{c_G} = \frac{\omega^2}{c^2} \mathbf{c_G} \tag{83}$$

This is an infinite set of equation for the set of unknown eigenvectors, $\mathbf{c_G}$. We can truncate it by only taking a finite amount of plane waves, where the problem is then reduced to a classical matrix eigenvalue problem, $Ax = \omega^2 x$. By recovering the associated frequency eigenvalues, we will have calculated the dispersion relation of the photonic crystal, along the points of high symmetry in the first Brillouin zone.

Bibliography

[1] Prachi Sharma, Rohit Arora, Suraj Pardeshi, and Mandeep Singh. Fibre optic communications: An overview. *International Journal of Emerging Technology and Advanced Engineering*, 3:474–479, 05 2013.

[2] Ott Scheler, Jared T. Kindt, Abraham J. Qavi, Lauris Kaplinski, Barry Glynn, Thomas Barry, Ants Kurg, and Ryan C. Bailey. Label-free, multiplexed detection of bacterial tmrna using silicon photonic microring resonators. *Biosensors & bioelectronics*, 36(1):56–61, 2012. 22541813[pmid].

[3] Vien Van. Circuit-based method for synthesizing serially coupled microring filters. *J. Lightwave Technol.*, 24(7):2912, Jul 2006.

[4] W. Bogaerts, P. D Heyn, T. V Vaerenbergh, K. D Vos, S. K Selvaraja, T. Claes, P. Dumon, P. Bienstman, D. V Thourhout, and R. Baets. Silicon microring resonators. *Laser & Photonics Reviews*, 6(1):47–73, 2012.

[5] A. Pimpin and W Srituravanich. Review on micro- and nanolithography techniques and their application. *Eng. J.*, 16(1):37–56, 2011.

[6] Lukas Chrostowski and Michael Hochberg. *Silicon Photonics Design: From Devices to Systems*. Cambridge University Press, 2015.

[7] M. Z. Hasan and C. L. Kane. Colloquium: Topological insulators. *Rev. Mod. Phys.*, 82:3045–3067, Nov 2010.

[8] Shuichi Murakami. Two-dimensional topological insulators and their edge states. 302:012019, jul 2011.

[9] Z. Wang, Y. Chong, J. D. Joannopoulos, and M. Soljaić. Observation of unidirectional backscattering-immune topological electromagnetic states. *Nature*, 461:772–775, 2009.

[10] W. P. Su, J. R. Schrieffer, and A. J. Heeger. Solitons in polyacetylene. *Phys. Rev. Lett.*, 42:1698–1701, Jun 1979.

[11] E. Hecht. *Optics*. Pearson education, 5th edition, 2017.

[12] F. Goos and H. Hänchen. Ein neuer und fundamentaler versuch zur totalreflexion. *Annalen der Physik*, 436(7-8):333–346, 1947.

[13] A .W. Snyder and J. Love. *Optical Waveguide Theory*. Springer, 1 edition, 1983.

[14] David J Griffiths. *Introduction to electrodynamics; 4th ed.* Pearson, Boston, MA, 2013. Re-published by Cambridge University Press in 2017.

[15] John David Jackson. *Classical electrodynamics; 2nd ed.* Wiley, New York, NY, 1975.

[16] Matthew R. Foreman, Jon D. Swaim, and Frank Vollmer. Whispering gallery mode sensors. *Adv. Opt. Photon.*, 7(2):168–240, Jun 2015.

[17] R. A. Waldron. Perturbation theory of resonant cavities. *Proceedings of the IEE - Part C: Monographs*, 107(12):272–274, 1960.

[18] Nur Ismail, Cristine Calil Kores, Dimitri Geskus, and Markus Pollnau. Fabry-perot resonator: spectral line shapes, generic and related airy distributions, linewidths, finesses, and performance at low or frequency-dependent reflectivity. *Opt. Express*, 24(15):16366–16389, Jul 2016.

[19] Andrey Matsko and Vladimir Ilchenko. Optical resonators with whispering-gallery mode-part i. *Selected Topics in Quantum Electronics, IEEE Journal of*, 12:3 – 14, 02 2006.

[20] Lin Gan and ZhiYuan Li. Photonic crystal cavities and integrated optical devices. *Science China Physics, Mechanics & Astronomy*, 58(11):114203, Oct 2015.

[21] V. Van. *Optical Microring Resonators: Theory, Techniques, and Applications*. Taylor & Francis, 2017.

[22] Jessica Steinlechner, Christoph Krueger, Nico Lastzka, Sebastian Steinlechner, Alexander Khalaidovski, and Roman Schnabel. Optical absorption measurements on crystalline silicon test masses at 1550 nm. *Classical and Quantum Gravity*, 30(9):095007, May 2013.

[23] A. Yariv. Coupled-mode theory for guided-wave optics. *IEEE Journal of Quantum Electronics*, 9(9):919–933, 1973.

[24] H. A. Haus and W. Huang. Coupled-mode theory. *Proceedings of the IEEE*, 79(10):1505–1518, 1991.

[25] S. Chuang. A coupled mode formulation by reciprocity and a variational principle. *Journal of Lightwave Technology*, 5:5–15, 1987.

[26] D.J. Griffiths. *Introduction to Quantum Mechanics*. Cambridge University Press, 3rd edition, 2018.

[27] N. W. Ashcroft and N. D. Mermin. *Solid State Physics*. Harcourt Brace College Publishers, 1976.

[28] J.D. Joannopoulos, S.G Johnson, J.N Winn, and R.D Meade. *Photonic Crystals: Molding the Flow of Light*. Princeton University Press, 2nd edition, 2007.

[29] K.F. Riley, M.P. Hobson, and S.J. Bence. *Mathematical Methods for Physics and Engineering: A Comprehensive Guide*. Cambridge University Press, 2006.

[30] M. Z. Hasan and C. L. Kane. Colloquium: Topological insulators. *Rev. Mod. Phys.*, 82:3045–3067, Nov 2010.

[31] Klaus von Klitzing. The quantized hall effect. *Rev. Mod. Phys.*, 58:519–531, Jul 1986.

[32] Di Xiao, Ming-Che Chang, and Qian Niu. Berry phase effects on electronic properties. *Rev. Mod. Phys.*, 82:1959–2007, Jul 2010.

[33] C. L. Kane and T. C. Lubensky. Topological boundary modes in isostatic lattices. *Nature Physics*, 10(1):39–45, Jan 2014.

[34] P. Delplace, D. Ullmo, and G. Montambaux. Zak phase and the existence of edge states in graphene. *Phys. Rev. B*, 84:195452, Nov 2011.

[35] János K. Asbóth, László Oroszlány, and András Pályi. A short course on topological insulators. *Lecture Notes in Physics*, 2016.

[36] Xiao-Liang Qi, Yong-Shi Wu, and Shou-Cheng Zhang. General theorem relating the bulk topological number to edge states in two-dimensional insulators. *Phys. Rev. B*, 74:045125, Jul 2006.

[37] Shinsei Ryu, Andreas P Schnyder, Akira Furusaki, and Andreas W W Ludwig. Topological insulators and superconductors: tenfold way and dimensional hierarchy. *New Journal of Physics*, 12(6):065010, Jun 2010.

[38] Tomoki Ozawa, Hannah M. Price, Alberto Amo, Nathan Goldman, Mohammad Hafezi, Ling Lu, Mikael C. Rechtsman, David Schuster, Jonathan Simon, Oded Zilberberg, and Iacopo Carusotto. Topological photonics. *Rev. Mod. Phys.*, 91:015006, Mar 2019.

[39] Yasutomo Ota, Kenta Takata, Tomoki Ozawa, Alberto Amo, Zhetao Jia, Boubacar Kante, Masaya Notomi, Yasuhiko Arakawa, and Satoshi Iwamoto. Active topological photonics. *Nanophotonics*, 9(3):547 – 567, 01 Mar. 2020.

[40] S. Raghu and F. D. M. Haldane. Analogs of quantum-hall-effect edge states in photonic crystals. *Phys. Rev. A*, 78:033834, Sep 2008.

[41] Midya Parto, Steffen Wittek, Hossein Hodaei, Gal Harari, Miguel A. Bandres, Jinhan Ren, Mikael C. Rechtsman, Mordechai Segev, Demetrios N. Christodoulides, and Mercedeh Khajavikhan. Edge-mode lasing in 1d topological active arrays. *Phys. Rev. Lett.*, 120:113901, Mar 2018.

[42] Yasutomo Ota, Ryota Katsumi, Katsuyuki Watanabe, Satoshi Iwamoto, and Yasuhiko Arakawa. Topological photonic crystal nanocavity laser. *Communications Physics*, 1(1):86, Nov 2018.

[43] Zhifeng Zhang, Mohammad Hosain Teimourpour, Jake Arkinstall, Mingsen Pan, Pei Miao, Henning Schomerus, Ramy El-Ganainy, and Liang Feng. Experimental realization of multiple topological edge states in a 1d photonic lattice. *Laser & Photonics Reviews*, 13(2):1800202, 2019.

[44] Ardavan Oskooi, David Roundy, Mihai Ibanescu, Peter Bermel, J.D. Joannopoulos, and Steven Johnson. Meep: A flexible free-software package for electromagnetic simulations by the fdtd method. *Computer Physics Communications*, 181:687–702, 03 2010.

[45] Kathleen McGarvey-Lechable and Pablo Bianucci. Maximizing slow-light enhancement in one-dimensional photonic crystal ring resonators. *Optics Express*, 22, 10 2014.

[46] Chris Mack. The new, new limits of optical lithography. *Proceedings of SPIE - The International Society for Optical Engineering*, 5374, 05 2004.

[47] Zhiyong Zhu, Yingchun Cheng, and Udo Schwingenschlögl. Band inversion mechanism in topological insulators: A guideline for materials design. *Phys. Rev. B*, 85:235401, Jun 2012.

[48] Chris Mack. The new, new limits of optical lithography. *Proceedings of SPIE - The International Society for Optical Engineering*, 5374, 05 2004.

[49] A. Farjadpour, David Roundy, Alejandro Rodriguez, M. Ibanescu, Peter Bermel, J. D. Joannopoulos, Steven G. Johnson, and G. W. Burr. Improving accuracy by subpixel smoothing in the finite-difference time domain. *Opt. Lett.*, 31(20):2972–2974, Oct 2006.

[50] DanXia Xu, André Delâge, Pavel Cheben, Boris Lamontagne, S. Janz, and Winnie Ye. Silicon-on-insulator (soi) as a photonics platform. *Proceedings - Electrochemical Society*, 01 2005.

[51] D. J. Blumenthal, R. Heideman, D. Geuzebroek, A. Leinse, and C. Roeloffzen. Silicon nitride in silicon photonics. *Proceedings of the IEEE*, 106(12):2209–2231, 2018.

[52] Yifang Chen. Nanofabrication by electron beam lithography and its applications: A review. *Microelectronic Engineering*, 135:57 – 72, 2015.

[53] G. L. . Chiu and J. M. Shaw. Optical lithography: Introduction. *IBM Journal of Research and Development*, 41(1.2):3–6, 1997.

[54] Lirong Cheng, Simei Mao, Zhi Li, Yaqi Han, and H. Y. Fu. Grating couplers on silicon photonics: Design principles, emerging trends and practical issues. *Micromachines*, 11(7), 2020.

[55] M. Hafezi, S. Mittal, J. Fan, A. Migdall, and J. M. Taylor. Imaging topological edge states in silicon photonics. *Nature Photonics*, 7(12):1001–1005, Dec 2013.

[56] Chia Wei Hsu, Bo Zhen, A.Douglas Stone, John Joannopoulos, and Marin Soljačić. Bound states in the continuum. *Nature Reviews Materials*, 1:16048, 07 2016.

[57] Luqi Yuan, Qian Lin, Meng Xiao, and Shanhui Fan. Synthetic dimension in photonics. *Optica*, 5(11):1396–1405, Nov 2018.

[58] Dominik Rabus. *Integrated Ring Resonators: The Compendium*, volume 127. 01 2007.

[59] Kane Yee. Numerical solution of initial boundary value problems involving maxwell's equations in isotropic media. *IEEE Transactions on Antennas and Propagation*, 14(3):302–307, 1966.

[60] Jean-Pierre Bérenger. Perfectly matched layer (pml) for computational electromagnetics. *Synthesis Lectures on Computational Electromagnetics*, 2:1–117, 01 2007.

[61] S. G. Johnson and J. D. Joannopoulos. Block-iterative frequency-domain methods for maxwell's equations in a planewave basis. *Opt. Express*, 8(3):173–190, Jan 2001.